

Casimir Energy of 5D Electromagnetism and New Regularization Based on Minimal Area Principle

S. Ichinose

January 10, 2019

*Laboratory of Physics, School of Food and Nutritional Sciences, University of Shizuoka
Yada 52-1, Shizuoka 422-8526, Japan*

Abstract

We examine the Casimir energy of 5D electromagnetism in the recent standpoint. The bulk geometry is flat. Z_2 symmetry and the periodic property, for the extra coordinate, are taken into account. After confirming the consistency with the past result, we do new things based on a *new regularization*. In the treatment of the divergences, we introduce IR and UV cut-offs and *restrict* the (4D momentum, extra coordinate)-integral region. The regularized configuration is the *sphere lattice*, in the 4D continuum space, which changes along the extra coordinate. The change (renormalization flow) is specified by the *minimal area principle*, hence this regularization configuration is string-like. We do the analysis not in the Kaluza-Klein expanded form but in a *closed* form. We do *not* use any perturbation. The formalism is based on the heat-kernel approach using the *position/momentum propagator*. Interesting relations between the heat-kernels and the P/M propagators are obtained, where we introduce the *generalized* P/M propagators. A useful expression of the Casimir energy, in terms of the P/M propagator, is obtained. The restricted-region approach is replaced by the weight-function approach in the latter-half description. Its meaning, in relation to the *space-time quantization*, is argued. *Finite* Casimir energy is numerically obtained. The compactification-size parameter (periodicity) suffers from the renormalization effect. Numerical evaluation is exploited. Especially the minimal surface lines in the 5D flat space are obtained both numerically using the Runge-Kutta method and analytically using the general solution.

PACS: PACS NO: 04.50.+h, 11.10.Kk, 11.25.Mj, 12.10.-g

Keywords: position/momentum propagator, Z_2 -parity, Randall-Schwartz, heat-kernel, Casimir energy, sphere lattice, minimal surface, 5 dimensional electromagnetism

1 Introduction

As a unified theory of the four forces in nature, the higher dimensional models have a long history since Kaluza-Klein[1, 2]. The simplest one unifies the forces of graviton, photon and

dilaton. The quantum effects are evaluated by Appelquist and Chodos[3]. They evaluated the Casimir energy¹ and the result has been giving us the standard image of the contraction of the extra space, that is, when the compactification takes place, the extra space shrinks to a small size slightly bigger than the Planck length.

The higher dimensional models have, at present, the defect that they, by themselves, are *unrenormalizable*. In Ref.[3], the UV divergence appears as the quintical divergence, Λ^5 , of the *cosmological term*. It simply means that we do not have a proper procedure to define physical quantities within the quantum field theory(QFT). One can, at this point, have the standpoint that they are effective theories which should be derived from the more fundamental models such as the string theory, M-theory or D-brane. In the present paper, we pursue the possibility that there is a proper procedure to define physical quantities within the higher dimensional QFT. We propose a procedure and show it works well.

There are some approaches to this problem. One is the deconstruction model[5, 6]. One discretize the extra coordinate and choose appropriate finite-number of "branes" keeping gauge invariance. This is a popular approach at present. Some interesting results are reported[7, 8]. The other approach is the one based on the regularization using the position-dependent cut-off[9]. The integral region is restricted appropriately. The restriction requirement comes from the analysis of the propagator behaviour[9, 10]. Spiritually the *holography* idea is behind. The present motivation comes from the question. "Can we find the reason why the restriction process is necessary within the framework of the 5D QFT, not using the string theory and related supergravity theories?"

We introduce a *new* regularization inspired by the partial success of the Randall-Schwartz's result. We associate the regularization (in 4D world) cut-offs running along the extra axis y , with the *minimal area surfaces* in the bulk. In this way, the string-like (surface) configuration (closed string) is introduced in the present approach. This is quite contrasting with the usual string theory approach. The present string-like configuration appears not from the propagation of strings but from the necessity of restriction of the integral region in the bulk space.

The original approach for the renormalization flow interpretation of the bulk behaviour relies on the AdS/CFT and 5D supergravity [13, 14, 15, 16, 17, 18]. The present approach does *not* rely on them. We *directly* use the minimal area principle, the essence of the string theory[19, 20, 21], in the *regularization procedure*. This is *new* in the development of the quantum field theory.

The paper content is as follows. In Sec.2, we review the 5D quantum electromagnetism in the recent standpoint. Casimir energy is obtained from the KK-expansion approach. In Sec.3, the same quantity of Sec.2 is dealt in the heat-kernel method and the Casimir energy is expressed in a closed form in terms of the P/M propagator. The closed expression of Casimir energy is numerically evaluated and its equivalence with the Sec.2's result is confirmed in Sec.4. Here we introduce UV and IR regularization parameters in (4D momentum, extra coordinate)-space. A new idea about the UV and IR regularization is presented in Sec.5. The minimal surface principle is introduced. The *sphere lattice*

¹ For a recent review, see ref.[4].

and the *renormalization* are explained. In Sec.6 an improved regularization procedure is presented where a *weight function* is introduced. Here again the *minimal surface principle* is taken. The definition of the weight function is given in Sec.7. In Sec.8 we make the concluding remarks. We prepare two appendices to supplement the text. App.A deals with the analytic solution of the minimal surface curve in the 5D flat space. App.B explains the numerical confirmation of the (approximate) equality of the minimal surface curve and the dominant path in the Casimir energy calculation.

2 Five Dimensional Quantum Electromagnetism

We consider the flat 5D space-time $(X^M) = (x^\mu, y)$ with the periodicity in the extra space y .

$$ds^2 = \eta_{\mu\nu} dx^\mu dx^\nu + dy^2 \quad , \quad -\infty < y < \infty \quad , \quad y \rightarrow y + 2l, \\ (\eta_{\mu\nu}) = \text{diag}(-1, 1, 1, 1) \quad , \quad (X^M) = (x^\mu, x^5 = y) \equiv (x, y) \quad , \quad M, N = 0, 1, 2, 3, 5; \quad \mu, \nu = 0, 1, 2, 3. \quad (1)$$

The 5D electromagnetism is described by the 5D U(1) gauge field A_M .

$$S_{EM} = \int d^4x dy \sqrt{-G} \left\{ -\frac{1}{4} F_{MN} F^{MN} \right\} \equiv \int d^4x dy \mathcal{L}_{EM} \quad , \quad G = \det G_{MN} \quad , \\ F_{MN} = \partial_M A_N - \partial_N A_M \quad , \quad (X^M) = (x^\mu, y) \quad , \\ ds^2 = G_{MN} dX^M dX^N \quad , \quad (G_{MN}) = \text{diag}(-1, 1, 1, 1, 1) \quad (2)$$

It has U(1) gauge symmetry.

$$A_M \rightarrow A_M + \partial_M \Lambda \quad , \quad (3)$$

where $\Lambda(X)$ is the 5D gauge parameter.

We respect Z_2 symmetry in the extra space.

$$y \rightarrow -y \quad . \quad (4)$$

The Z_2 parity assignment of $A_M(x^\mu, y)$ is fixed by the 5D gauge transformation (3). There are two cases corresponding to the choice of the Z_2 parity of $\Lambda(x^\mu, y)$.

$$\begin{aligned} \text{Case 1. Even parity case} \quad \Lambda(x^\mu, y) &= +\Lambda(x^\mu, -y) \\ A_\mu : P &= + \quad , \quad A_5 : P = - \\ \text{Case 2. Odd parity case} \quad \Lambda(x^\mu, y) &= -\Lambda(x^\mu, -y) \\ A_\mu : P &= - \quad , \quad A_5 : P = + \quad . \end{aligned} \quad (5)$$

In the present paper, we consider the Case 1. (Case 2 can be similarly treated.)

We take the following gauge-fixing term to quantize the present system.²

$$\begin{aligned}\mathcal{L}_g &= -\frac{1}{2}(\partial_M A^M)^2 = -\frac{1}{2}(\partial_\mu A^\mu + \partial_y A^5)^2 \quad , \\ \mathcal{L}_{EM} + \mathcal{L}_g &= \frac{1}{2}A_\mu(\partial^2 + \partial_y^2)A^\mu + \frac{1}{2}A^5(\partial^2 + \partial_y^2)A^5 + \text{total derivatives} \quad ,\end{aligned}\quad (6)$$

where $\partial^2 \equiv \partial_\mu \partial^\mu$. Then the field equations are given by

$$(\partial^2 + \partial_y^2)A^\mu = 0 \quad , \quad (\partial^2 + \partial_y^2)A^5 = 0 \quad . \quad (7)$$

We consider the system in the periodic condition (1). Then we can write as

$$\begin{aligned}A^\mu(x, y) &= a_0^\mu(x) + 2 \sum_{n=1}^{\infty} a_n^\mu(x) \cos \frac{n\pi}{l} y \quad , \quad P=+ \\ A^5(x, y) &= 2 \sum_{n=1}^{\infty} b_n(x) \sin \frac{n\pi}{l} y \quad , \quad P=- \quad ,\end{aligned}\quad (8)$$

where $\{a_n^\mu(x)\}$ and $\{b_n(x)\}$ are the KK-expansion coefficients. From (7), they satisfy

$$\partial^2 a_0^\mu = 0 \quad (\text{zero mode}) \quad , \quad \{\partial^2 - (\frac{n\pi}{l})^2\}a_n^\mu = 0 \quad , \quad \{\partial^2 - (\frac{n\pi}{l})^2\}b_n = 0 \quad , \quad n \neq 0 \quad . \quad (9)$$

The on-shell condition, (7) or (9), is for the analysis of S-matrix. In this paper, we do not use the condition.³ The total action can be written by

$$\int_{-l}^l dy (\mathcal{L}_{EM} + \mathcal{L}_g) = 2l \left\{ \frac{1}{2} \sum_{n \in \mathbf{Z}} a_{n\mu} (\partial^2 - (\frac{n\pi}{l})^2) a_n^\mu + \frac{1}{2} \sum_{n \in \mathbf{Z}, n \neq 0} b_n (\partial^2 - (\frac{n\pi}{l})^2) b_n \right\} \quad . \quad (11)$$

² The gauge-independence of the physical quantities is an important check point of the proposal of the present paper. We relegate it to a future work. The gauge-independence of the Casimir energy of the 5D KK-theory (Appelquist and Chodos's result[3]) was confirmed in Ref.[22].

³ We do not take into account the degree of freedom 5-2=3 among 5 components $\{A^M\}$ due to the local gauge symmetry. This is because we will compare the present results of the flat geometry with those of the warped geometry. In the latter treatment we start with the *massive* vector theory which does *not* have the local gauge symmetry.[9]

$$S_{5dV} = \int d^4 x dz \sqrt{-G} \left(-\frac{1}{4} F_{MN} F^{MN} - \frac{1}{2} m^2 A^M A_M \right) \quad , \quad . \quad (10)$$

The 5D mass parameter m is regarded as an IR-regularization parameter. The 5D gauge theory is the limit $m = 0$. For the general m , the Csimir energy is some integral of the (modified) Bessel functions with the number $\nu = \sqrt{1 + m^2/\omega^2}$ where ω is the warp parameter. The most simplest case, for the analysis, is not $m = 0$ but $m = i\omega$. The UV-behaviour, which is the key point of the present paper, is cosidered independent of the IR regularization parameter m . Hence the massive case is (practically) important for the 5D theories. We also include the longitudinal component to respect the manifest 5D Lorentz invariance. For the later use of the comparison with the warped case, we consider , instead of the 5D EM, the system of four 5D massless scalars with the even-parity and one with the odd-parity.

Then the Casimir energy E_{Cas} is given by ⁴

$$\begin{aligned} e^{-l^4 E_{Cas}} &= \int \prod_{n,\mu} \mathcal{D}a_n^\mu \prod_{m \neq 0} db_m \exp i \int d^4x dy (\mathcal{L}_{EM} + \mathcal{L}_g) \\ &= \exp \left[-\frac{1}{2} l^4 \int \frac{d^4p}{(2\pi)^4} \left\{ 4 \sum_{n \in \mathbf{Z}} \ln(p^2 + m_n^2) + \sum_{n \in \mathbf{Z}, n \neq 0} \ln(p^2 + m_n^2) \right\} \right] , \end{aligned} \quad (12)$$

where $p^2 \equiv p_\mu p^\mu$ and $m_n = \frac{n\pi}{l}$. This expression is the standard one. The above KK-summation and p_μ integral are divergent, hence we must regularize them. The standard way, taken by Appelquist and Chodos[3], goes as follows. It is sufficient to consider the even-parity quantity below.

$$V(l) = \frac{1}{2} \int \frac{d^4p}{(2\pi)^4} \sum_{n \in \mathbf{Z}} \ln(p^2 + m_n^2) \quad . \quad (13)$$

This is the (unregularized) Casimir energy for one scalar mode with Z_2 -parity even. First step is to introduce a reference point l_0 .

$$V(l) - V(l_0) = \frac{1}{2} \int \frac{d^4p}{(2\pi)^4} \sum_{n \in \mathbf{Z}} \ln \frac{(p^2 + (\frac{n\pi}{l})^2)}{(p^2 + (\frac{n\pi}{l_0})^2)} \quad . \quad (14)$$

This procedure makes us drop the l -independent quantity. Using the well-known formula

$$\sum_{n=-\infty}^{\infty} f_n = \int_{-\infty}^{\infty} dz f(z) + \int_{-\infty+i\epsilon}^{+\infty+i\epsilon} dz \frac{f(z) + f(-z)}{e^{-2\pi iz} - 1} \quad , \quad (15)$$

the KK-sum in (14) is replaced by the z -integral:

$$V(l) - V(l_0) = \frac{1}{2} \int \frac{d^4p}{(2\pi)^4} \left[\int_{-\infty}^{\infty} dz \ln \frac{p^2 + (\frac{z\pi}{l})^2}{p^2 + (\frac{z\pi}{l_0})^2} + \int_{-\infty+i\epsilon}^{+\infty+i\epsilon} dz \frac{2 \ln \frac{p^2 + (\frac{z\pi}{l})^2}{p^2 + (\frac{z\pi}{l_0})^2}}{e^{-2\pi iz} - 1} \right] \quad . \quad (16)$$

We consider the space-like 4D momentum p_μ : $p^2 = p_\mu p^\mu > 0$. Using the second formula:

$$\int_{-\infty}^{\infty} dz H(z) \ln \frac{z^2 + a^2}{z^2 + b^2} = 2\pi \int_b^a dx H(ix) \quad , \quad (17)$$

the first part of (16) is evaluated as

$$\frac{1}{2} \int \frac{d^4p}{(2\pi)^4} \int_{-\infty}^{\infty} dz \ln \frac{(p^2 + (\frac{z\pi}{l})^2)}{(p^2 + (\frac{z\pi}{l_0})^2)} = (l - l_0) \int \frac{d^4p}{(2\pi)^4} \sqrt{p^2} \quad . \quad (18)$$

⁴ The Casimir energy is defined to be the free part (independent of the coupling) of the vacuum energy which depends on the *boundary*. The quantity is defined to be the energy per unit space-volume of the "brane". In the present model of 3-brane (3+1 dim real world), the space-volume has the dimension of L^3 . Hence the dimension of E_{Cas} is L^{-4} .

This integral is quintically divergent, but turns out to be cancelled out as shown below. As for the second part, the integrand of the p-integral, using the formula (17) again, is evaluated as

$$\begin{aligned} \int_{-\infty}^{\infty} dz \frac{\ln \frac{(p^2 + (\frac{z\pi}{l_0})^2)}{(p^2 + (\frac{z\pi}{l})^2)}}{e^{-2\pi iz} - 1} &= 2\pi \int_{\frac{l_0}{\pi}\sqrt{p^2}}^{\frac{l}{\pi}\sqrt{p^2}} \frac{1}{e^{2\pi x} - 1} dx \\ &= -\sqrt{p^2}(l - l_0) + \ln \frac{e^{l\sqrt{p^2}} - e^{-l\sqrt{p^2}}}{e^{l_0\sqrt{p^2}} - e^{-l_0\sqrt{p^2}}} . \end{aligned} \quad (19)$$

We see the first term in the above final expression, after the p-integral, cancel the quintically divergent one (18). Hence we finally obtain

$$\begin{aligned} V(l) - V(l_0) &= \int \frac{d^4 p}{(2\pi)^4} \ln \frac{e^{l\sqrt{p^2}} - e^{-l\sqrt{p^2}}}{e^{l_0\sqrt{p^2}} - e^{-l_0\sqrt{p^2}}} \\ &= \frac{1}{8\pi^2} \frac{1}{l^4} \int_0^\infty dk k^3 \{k + \ln(1 - e^{-2k}) - \frac{l_0}{l} k - \ln(1 - e^{-\frac{2l_0}{l}k})\} , \quad (l\sqrt{p^2} \equiv k) . \end{aligned} \quad (20)$$

Using the third formula

$$\int_0^\infty dk k^3 \ln(1 - e^{-2k}) = -\frac{3}{4}\zeta(5) , \quad (21)$$

we obtain

$$8\pi^2[V(l) - V(l_0)] = (1 - \frac{l_0}{l}) \frac{1}{l^4} \int_0^\infty dk k^4 + \frac{1}{l^4} \{-\frac{3}{4}\zeta(5) + (\frac{l}{l_0})^4 \cdot \frac{3}{4} \cdot \zeta(5)\} . \quad (22)$$

The first term is *quintically* divergent. We take, as the (dimensionless) UV *cut-off* of the k -integral, $l\Lambda$, then

$$8\pi^2[V(l) - V(l_0)] = \frac{1}{5}l\Lambda^5 - \frac{3}{4}\frac{\zeta(5)}{l^4} - (\frac{1}{5}l_0\Lambda^5 - \frac{3}{4}\frac{\zeta(5)}{(l_0)^4}) . \quad (23)$$

Hence we obtain the Casimir energy and the Casimir force for the simple system (13) as

$$\begin{aligned} 8\pi^2 \times V(l) &= \frac{1}{5}l\Lambda^5 - \frac{3}{4}\frac{\zeta(5)}{l^4} , \quad F_{Cas}^\Lambda(l) = -\frac{\partial V}{\partial l} = \left(-\frac{1}{5}\Lambda^5 - 3\frac{\zeta(5)}{l^5}\right) \frac{1}{8\pi^2} , \\ &\quad \zeta(5) = 1.03693 \dots . \end{aligned} \quad (24)$$

The first term of $V(l)$ is *quintically* divergent but is simply proportional to l . This quantity comes from the *UV-divergences* of 5D quantum fluctuation. In the Casimir force $F_{Cas}^\Lambda = -\frac{\partial V}{\partial l}$, that part does not depend on l . If we can find a right way to avoid the UV-divergences (which will be proposed later) we may drop the (divergent) constant contribution, and we obtain the Casimir force for the 5D electromagnetism as

$$F_{Cas} = 5 \times \left(-3\frac{\zeta(5)}{l^5}\right) \times \frac{1}{8\pi^2} . \quad (25)$$

The minus sign means the *attractive* force.

3 Heat-Kernel Approach and Position/Momentum Propagator

We reformulate the previous section using the heat-kernel in order to treat the problem *without* KK-expansion. Note that the heat-kernel method is a complete quantization procedure for the free theory (quadratic theory)[23]. Instead of the 5D gauge fields $A^M(X)$, we introduce partially-Fourier-transformed ones $A_p^M(y) = (A_p^\mu(y), B_p(y))$.

$$\begin{aligned} A^\mu(x, y) &= \int \frac{d^4 p}{(2\pi)^4} e^{ipx} A_p^\mu(y) \quad : \quad P=+ \\ A^5(x, y) &= \int \frac{d^4 p}{(2\pi)^4} e^{ipx} B_p(y) \quad : \quad P=- \end{aligned} \quad (26)$$

(We do *not* Fourier-transform the extra space (y) part.) Then the total action is given by

$$S = \int d^4 x dy (\mathcal{L}_{EM} + \mathcal{L}_g) = \int \frac{d^4 p}{(2\pi)^4} \int_{-l}^l dy \left[\frac{1}{2} A_{\mu p}(y) (-p^2 + \partial_y^2) A_p^\mu(y) + \frac{1}{2} B_p(y) (-p^2 + \partial_y^2) B_p(y) \right] \quad (27)$$

Here we restrict the y-integral region to $[-l, l]$ because it has a sufficient information and can be transformed (by the Fourier expansion) to the periodic form defined in $(-\infty, +\infty)$. The on-shell condition is given by

$$\begin{aligned} (-p^2 + \partial_y^2) A_p^\mu(y) &= 0 \quad , \quad -l \leq y \leq l \quad , \quad P=+ \\ (-p^2 + \partial_y^2) B_p(y) &= 0 \quad , \quad -l \leq y \leq l \quad , \quad P=- \end{aligned} \quad (28)$$

This condition, which is *not* used in the following, is necessary when we consider S-matrix. The Casimir energy E_{Cas} is given by

$$e^{-l^4 E_{Cas}} = \int \mathcal{D}A_{\mu p} \mathcal{D}B_p \exp\{iS\} = \exp l^4 \int \frac{d^4 p}{(2\pi)^4} \frac{1}{2l} \int_{-l}^l dy \left\{ -\frac{4}{2} \ln(p^2 - \partial_y^2) - \frac{1}{2} \ln(p^2 - \partial_y^2) \right\} \quad (29)$$

Using the formula [23]

$$\int_0^\infty \frac{e^{-t} - e^{-tM}}{t} dt = \ln M \quad , \quad \det M > 0 \quad , \quad M : \text{a matrix} \quad , \quad (30)$$

we can *formally* write as

$$-\ln(p^2 - \partial_y^2) = \int_0^\infty \frac{1}{t} e^{-t(p^2 - \partial_y^2)} dt + \text{divergent constant} \quad , \quad (31)$$

where the divergent constant should not depend on p and y . We understand M in (30) is the matrix $M_{y,y'}$ labeled by the continuous parameters y and y' and $(p^2 - \partial_y^2)$ in (31) is

the differential operator acting on $|y\rangle$, a quantum state labeled by the position y .⁵ The heat kernels H_p and E_p are, in the abstract way, defined by

$$\begin{aligned} H_p(y, y'; t) &= \langle y | e^{-(p^2 - \partial_y^2)t} | y' \rangle \Big|_{P=-} , \\ E_p(y, y'; t) &= \langle y | e^{-(p^2 - \partial_y^2)t} | y' \rangle \Big|_{P=+} . \end{aligned} \quad (32)$$

Hence we obtain the final expression of E_{Cas} .

$$e^{-l^4 E_{Cas}} = (\text{const}) \times \exp \left[l^4 \int \frac{d^4 p}{(2\pi)^4} \int_0^\infty \frac{dt}{t} \left\{ \frac{4}{2} \text{Tr } E_p(y, y'; t) + \frac{1}{2} \text{Tr } H_p(y, y'; t) \right\} \right] , \quad (33)$$

where Tr means the integral over all $y = y'$.⁶

$$\text{Tr } E_p(y, y'; t) = \int_{-l}^l dy E_p(y, y; t) , \quad \text{Tr } H_p(y, y'; t) = \int_{-l}^l dy H_p(y, y; t) . \quad (36)$$

The precise definition of H_p and E_p is given by, with the initial condition (39) shown later, the *heat equations*.

$$\begin{aligned} \left\{ \frac{\partial}{\partial t} + p^2 - \partial_y^2 \right\} H_p(y, y'; t) &= 0 , \quad P = - , \\ \left\{ \frac{\partial}{\partial t} + p^2 - \partial_y^2 \right\} E_p(y, y'; t) &= 0 , \quad P = + . \end{aligned} \quad (37)$$

The solutions are, in terms of the KK-eigen-functions, given by

$$\begin{aligned} H_p(y, y'; t) &= \frac{1}{2l} \sum_{n \in \mathbf{Z}} e^{-(k_n^2 + p^2)t} \frac{1}{2} \{ e^{-ik_n(y-y')} - e^{-ik_n(y+y')} \} , \\ E_p(y, y'; t) &= \frac{1}{2l} \sum_{n \in \mathbf{Z}} e^{-(k_n^2 + p^2)t} \frac{1}{2} \{ e^{-ik_n(y-y')} + e^{-ik_n(y+y')} \} , \\ k_n &= \frac{n\pi}{l} , \end{aligned} \quad (38)$$

⁵ $\langle y |$ and $|y\rangle$ are introduced by Dirac[24] and are called bra-vector and ket-vector respectively. It is defined by the orthonormal eigen functions of the kinetic differential operator of the system. When we take the orthogonality relation $\langle y | y' \rangle = \hat{\delta}(y - y')$, their physical dimensions are $[|y\rangle] = L^{-\frac{1}{2}}, [\langle y|] = L^{-\frac{1}{2}}$.

⁶ For the 5D free scalar with Z_2 -parity even, the Casimir Energy is given by

$$e^{-l^4 E_{Cas}} = (\text{const}) \times \exp \left[l^4 \int \frac{d^4 p}{(2\pi)^4} \int_0^\infty \frac{dt}{t} \frac{1}{2} \text{Tr } E_p(y, y'; t) \right] , \quad (34)$$

and, for that with Z_2 -parity odd,

$$e^{-l^4 E_{Cas}} = (\text{const}) \times \exp \left[l^4 \int \frac{d^4 p}{(2\pi)^4} \int_0^\infty \frac{dt}{t} \frac{1}{2} \text{Tr } H_p(y, y'; t) \right] , \quad (35)$$

where we have used the dimensionality of H_p and E_p read from (33); $[E_p]=[H_p]=L^{-1}$.⁷ The above heat-kernels satisfy the following b.c..

$$\begin{aligned}\lim_{t \rightarrow +0} H_p(y, y'; t) &= \frac{1}{2l} \sum_{n \in \mathbf{Z}} \frac{1}{2} \{e^{-ik_n(y-y')} - e^{-ik_n(y+y')}\} = \frac{1}{2} \{\hat{\delta}(y-y') - \hat{\delta}(y+y')\} \quad , \\ \lim_{t \rightarrow +0} E_p(y, y'; t) &= \frac{1}{2l} \sum_{n \in \mathbf{Z}} \frac{1}{2} \{e^{-ik_n(y-y')} + e^{-ik_n(y+y')}\} = \frac{1}{2} \{\hat{\delta}(y-y') + \hat{\delta}(y+y')\} \quad , \quad (39)\end{aligned}$$

where we have introduced $\hat{\delta}(y) \equiv \frac{1}{2l} \sum_{n \in \mathbf{Z}} e^{-ik_n y}$. With this b.c., the heat equation (37) can *rigorously* define H_p and E_p . We here introduce the *position/momentum propagators* G_p^\mp as follows.

$$\begin{aligned}G_p^-(y, y') &\equiv \int_0^\infty dt H_p(y, y'; t) = \frac{1}{2l} \sum_{n \in \mathbf{Z}} \frac{1}{k_n^2 + p^2} \frac{1}{2} \{e^{-ik_n(y-y')} - e^{-ik_n(y+y')}\} \quad , \\ G_p^+(y, y') &\equiv \int_0^\infty dt E_p(y, y'; t) = \frac{1}{2l} \sum_{n \in \mathbf{Z}} \frac{1}{k_n^2 + p^2} \frac{1}{2} \{e^{-ik_n(y-y')} + e^{-ik_n(y+y')}\} \quad , \quad (40)\end{aligned}$$

They satisfy the following differential equations of *propagators*.

$$(p^2 - \partial_y^2) G_p^\mp(y, y') = \frac{1}{2l} \sum_{n \in \mathbf{Z}} \frac{1}{2} \{e^{-ik_n(y-y')} \mp e^{-ik_n(y+y')}\} \equiv \frac{1}{2} \{\hat{\delta}(y-y') \mp \hat{\delta}(y+y')\} \quad , \quad (41)$$

Therefore the Casimir energy E_{Cas} is, from (33) and (38), given by

$$\begin{aligned}E_{Cas}(l) &= \int \frac{d^4 p}{(2\pi)^4} \int_0^\infty \frac{dt}{t} 2 \int_0^l dy \left\{ \frac{1}{2} \frac{1}{2l} \sum_{n \in \mathbf{Z}} e^{-(k_n^2 + p^2)t} \frac{1}{2} \{1 - e^{-2ik_n y}\} \right. \\ &\quad \left. + 2 \frac{1}{2l} \sum_{n \in \mathbf{Z}} e^{-(k_n^2 + p^2)t} \frac{1}{2} \{1 + e^{-2ik_n y}\} \right\} \quad . \quad (42)\end{aligned}$$

This expression leads to the same treatment as the previous section.

⁷ If we ignore the dimensionality,

$$\frac{1}{2l} \sum_{n \in \mathbf{Z}} \{e^{-(k_n^2 + p^2)t} / (k_n^2 + p^2)^s\} \frac{1}{2} \{e^{-ik_n(y-y')} \mp e^{-ik_n(y+y')}\}, \quad s : \text{ real number}$$

are the more general solutions of (37).

Here we introduce the *generalized* P/M propagators, $I_\alpha(P=-)$ and $J_\alpha(P=+)$ as

$$\begin{aligned}
I_\alpha(p^2; y, y') &\equiv \int_0^\infty \frac{dt}{t^\alpha} H_p(y, y'; t) \\
&= \int_0^\infty \frac{dt}{t^\alpha} \frac{1}{2l} \sum_{n \in \mathbf{Z}} e^{-(k_n^2 + p^2)t} \frac{1}{2} \{e^{-ik_n(y-y')} - e^{-ik_n(y+y')}\} \quad , \quad P=- \quad , \\
J_\alpha(p^2; y, y') &\equiv \int_0^\infty \frac{dt}{t^\alpha} E_p(y, y'; t) \\
&= \int_0^\infty \frac{dt}{t^\alpha} \frac{1}{2l} \sum_{n \in \mathbf{Z}} e^{-(k_n^2 + p^2)t} \frac{1}{2} \{e^{-ik_n(y-y')} + e^{-ik_n(y+y')}\} \quad , \quad P=+ \quad , \quad (43)
\end{aligned}$$

where α is the arbitrary real number. Then we have the following relations.

$$\begin{aligned}
I_0(p^2; y, y') &= G_p^-(y, y') \quad , \quad J_0(p^2; y, y') = G_p^+(y, y') \quad , \\
\frac{\partial I_\alpha(p^2; y, y')}{\partial p^2} &= -I_{\alpha-1}(p^2; y, y') \quad , \quad \int_{p^2}^\infty dk^2 I_\alpha(k^2; y, y') = I_{\alpha+1}(p^2; y, y') \quad , \\
\frac{\partial J_\alpha(p^2; y, y')}{\partial p^2} &= -J_{\alpha-1}(p^2; y, y') \quad , \quad \int_{p^2}^\infty dk^2 J_\alpha(k^2; y, y') = J_{\alpha+1}(p^2; y, y') \quad , \\
(p^2 - \partial_y^2) I_\beta(p^2; y, y') &= -\beta I_{\beta+1}(p^2; y, y') \quad , \quad (p^2 - \partial_y^2) J_\beta(p^2; y, y') = -\beta J_{\beta+1}(p^2; y, y') \quad , \quad \beta \neq 0 \quad .(44)
\end{aligned}$$

Finally we obtain the following useful expression of the Casimir energy in terms of P/M propagators.

$$\begin{aligned}
E_{Cas}(l) &= \int \frac{d^4 p}{(2\pi)^4} \left\{ \frac{1}{2} \text{Tr } I_1(p^2; y, y') + \frac{4}{2} \text{Tr } J_1(p^2; y, y') \right\} \\
&= \int \frac{d^4 p}{(2\pi)^4} \int_{p^2}^\infty \left\{ \frac{1}{2} \text{Tr } I_0(k^2; y, y') + 2 \text{Tr } J_0(k^2; y, y') \right\} dk^2 \\
&= \int \frac{d^4 p}{(2\pi)^4} \int_{p^2}^\infty \left\{ \frac{1}{2} \text{Tr } G_k^-(y, y') + 2 \text{Tr } G_k^+(y, y') \right\} dk^2 \quad . \quad (45)
\end{aligned}$$

Here we list the dimensions of various quantities appeared above.

Dim	$L^{1-2\alpha}$	L^{-4}	$L^{-3/2}$	L^{-1}	$L^{-1/2}$	L	L^2	$L^{5/2}$
	I_α, J_α	E_{Cas}	A^μ, A^5	μ, Λ, p H_p, E_p		ϵ, l, y G_p^\mp	t	A_p^μ, B_p
				$\hat{\delta}(y-y')$	$ y >, < y $			

(Λ, μ, ϵ are the regularization parameters defined below.)

The P/M propagators G_k^\mp , which is expressed in (40) in the form of summation over *all* modes, can be expressed in a *closed* form. (See, for example, [10].)

$$G_k^\mp(y, y') = \pm \frac{\cosh \tilde{k}(|y+y'| - l) \mp \cosh \tilde{k}(|y-y'| - l)}{4\tilde{k} \sinh \tilde{k}l} \quad , \quad -l \leq y \leq l \quad , \quad -l \leq y' \leq l$$

$$\tilde{k} \equiv \sqrt{k_\mu k^\mu} \quad , \quad k_\mu k^\mu > 0 (\text{space-like}) \quad , (46)$$

where the plural sign means that one corresponds to the other in the same position.⁸ The Casimir energy is, using the above results, explicitly written as

$$\begin{aligned}
E_{Cas}(l) &= \int \frac{d^4 p}{(2\pi)^4} \int_0^l dy (F^-(\tilde{p}, y) + 4F^+(\tilde{p}, y)) \quad , \\
F^-(\tilde{p}, y) &\equiv \int_{p^2}^{\infty} dk^2 G_k^-(y, y) = \int_{\tilde{p}}^{\infty} d\tilde{k} \frac{\cosh \tilde{k}(2y - l) - \cosh \tilde{k}l}{2 \sinh(\tilde{k}l)} \quad , \\
F^+(\tilde{p}, y) &\equiv \int_{p^2}^{\infty} dk^2 G_k^+(y, y) = \int_{\tilde{p}}^{\infty} d\tilde{k} \frac{-\cosh \tilde{k}(2y - l) - \cosh \tilde{k}l}{2 \sinh(\tilde{k}l)} \quad .
\end{aligned} \tag{47}$$

This is the closed expression, not the expanded one. (In relation to the degree of freedom of the system, the integrands of F^\pm are, in the later description, graphically shown in Fig.5 and Fig.6.)

4 UV and IR Regularization Parameters and Evaluation of Casimir Energy

The integral region of the equation (47) is displayed in Fig.1. In the figure, we introduce the *UV and IR regularization cut-offs*, $\mu \leq \tilde{p} \leq \Lambda$, $\epsilon \leq y \leq l$. In order to suppress the number of artificial parameters as much as possible, we take the relations⁹ :

$$\epsilon = \frac{1}{\Lambda} \quad , \quad \mu = \frac{1}{l} \quad . \tag{48}$$

This is the same situation as the *lattice gauge theory* (the unit lattice size = $(1/\Lambda)^4 \times \epsilon = (1/\Lambda)^5$, the total lattice size = $(1/\mu)^4 \times l = l^5$).

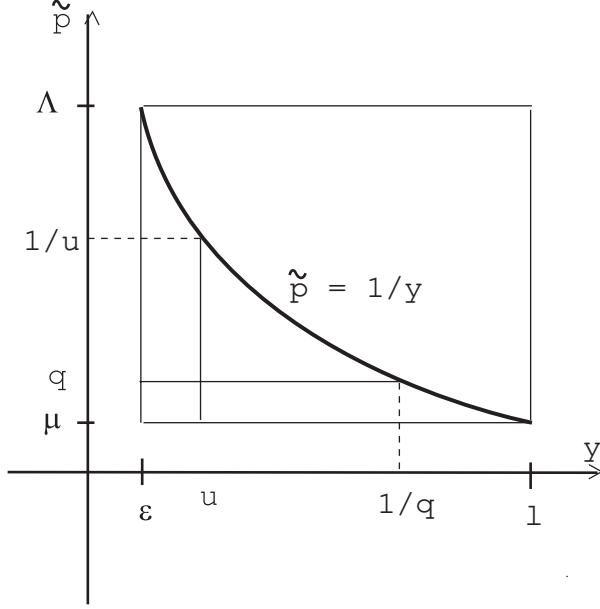
Let us evaluate the (Λ, l) -regularized value of (47).

$$\begin{aligned}
E_{Cas}(\Lambda, l) &= \frac{2\pi^2}{(2\pi)^4} \int_{1/l}^{\Lambda} d\tilde{p} \int_{1/\Lambda}^l dy \tilde{p}^3 F(\tilde{p}, y) \quad , \\
F(\tilde{p}, y) &\equiv F^-(\tilde{p}, y) + 4F^+(\tilde{p}, y) = \int_{\tilde{p}}^{\Lambda} d\tilde{k} \frac{-3 \cosh \tilde{k}(2y - l) - 5 \cosh \tilde{k}l}{2 \sinh(\tilde{k}l)} \quad .
\end{aligned} \tag{49}$$

⁸ The expression (46) is considered in $-l \leq y \leq l$, and the periodicity ($y \rightarrow y + 2l$) seems lost. If, however, we *Fourier-expand* (46) in the interval, the same expression as (40) is obtained. Note that the present treatment is crucially different from the deconstruction approach in that *all* Kaluza-Klein modes are taken into account. The necessity of the all KK modes was stressed in the $\delta(0)$ -problem of the bulk-boundary theory.[25, 26]

⁹ As for the numerical values of Λ and l , they depend on the chosen energy unit (such as eV, J, etc.) and the physical model concerned. For example, if we consider the grand unified theories, $\Lambda = 10^{19}$ GeV (Planck energy) and $l^{-1} = 10^3$ GeV (TeV physics) are strong candidates. Another case is the cosmological model. Then we take $\Lambda = 10^{19}$ GeV and $l^{-1} = 10^{-41}$ GeV ([Cosmological Size] $^{-1}$). Λ and l are huge numerical numbers in the application to the real world.

Figure 1: Space of (y, \tilde{p}) for the integration. The hyperbolic curve will be used in Sec.5.



The integral region of (\tilde{p}, y) is the *rectangle* shown in Fig.1. We now use the formula of the indefinite integrals:

$$\int \frac{\cosh(ax)}{\sinh x} dx = -\frac{e^{-(1-a)x}}{1-a} {}_2F_1\left(\frac{1-a}{2}, 1; \frac{3-a}{2}; e^{-2x}\right) - \frac{e^{-(1+a)x}}{1+a} {}_2F_1\left(\frac{1+a}{2}, 1; \frac{3+a}{2}; e^{-2x}\right) \quad ,$$

$$x > 0 \quad , \quad 1 > a \geq 0 \quad , (50)$$

where ${}_2F_1(\alpha, \beta; \gamma; z)$ is the Gauss's hypergeometric function. The formula below goes to the above one in the limit $a \rightarrow 1 - 0$ (ignoring the divergent constant $1/(a-1)$). The integrand of $E_{Cas}(\Lambda, l)$ (49), $\tilde{p}^3 F(\tilde{p}, y)$, can be *exactly* evaluated as

$$\begin{aligned} \tilde{p}^3 F(\tilde{p}, y) = & -\frac{\tilde{p}^3}{l} \left[-\frac{3}{2} \frac{e^{-(1-a(y))x}}{1-a(y)} {}_2F_1\left(\frac{1-a(y)}{2}, 1; \frac{3-a(y)}{2}; e^{-2x}\right) \right. \\ & \left. -\frac{3}{2} \frac{e^{-(1+a(y))x}}{1+a(y)} {}_2F_1\left(\frac{1+a(y)}{2}, 1; \frac{3+a(y)}{2}; e^{-2x}\right) + \frac{5}{2} \ln \sinh(x) \right]_{x=\tilde{p}l}^{x=\Lambda l} \quad , \\ & a(y) \equiv |2\frac{y}{l} - 1| \quad , \quad \Lambda^{-1} \leq y < l \quad , \quad l^{-1} \leq \tilde{p} \leq \Lambda \quad . \end{aligned} \quad (51)$$

Note that eq.(49), with (51), is the *rigorous* expression of the (Λ, l) -regularized Casimir energy. We show the behaviour of $\tilde{p}^3 F(\tilde{p}, y)$ taking the unit $l = 1$ in Fig.2-4. Three graphs correspond to $\Lambda = 10, 100, 1000$. All three graphs have a common shape. Behaviour along \tilde{p} -axis does not so much depend on y . A valley 'runs' parallel to the y -axis with the bottom

Figure 2: Behaviour of $\tilde{p}^3 F(\tilde{p}, y)$ (51). $l = 1$, $\Lambda = 10$, $0.1 \leq y < 1$, $1 \leq \tilde{p} \leq 10$.

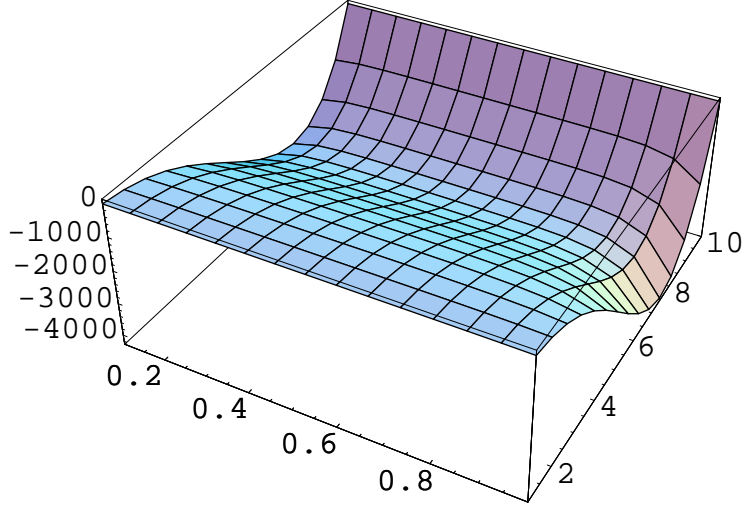


Figure 3: Behaviour of $\tilde{p}^3 F(\tilde{p}, y)$ (51). $l = 1$, $\Lambda = 100$, $0.01 \leq y < 1$, $1 \leq \tilde{p} \leq 100$.

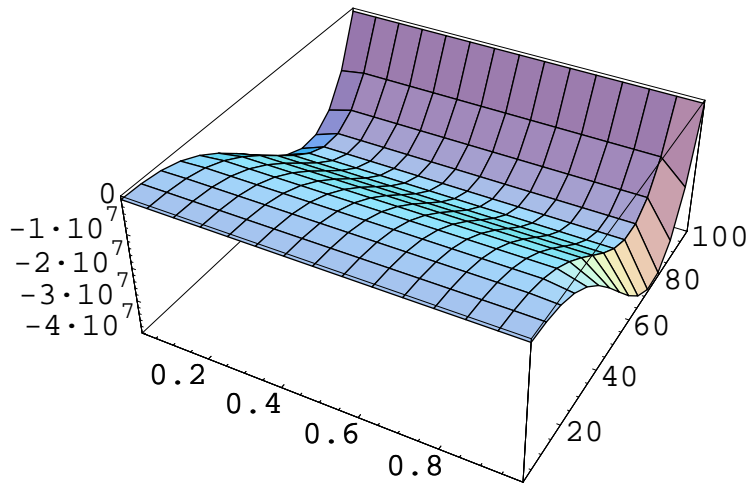
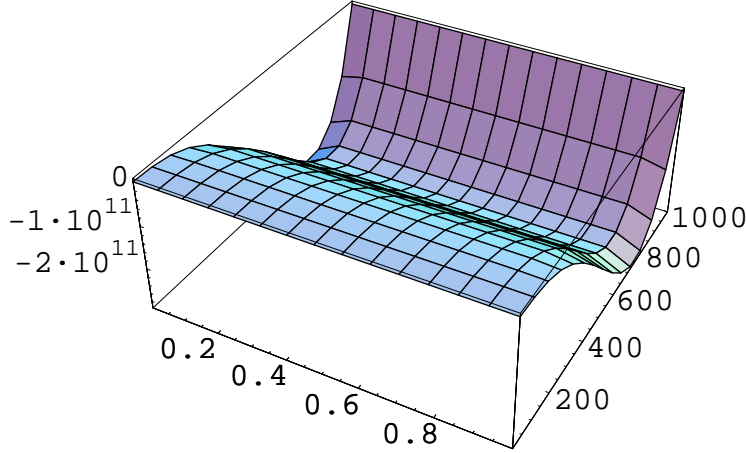


Figure 4: Behaviour of $\tilde{p}^3 F(\tilde{p}, y)$ (51). $l = 1$, $\Lambda = 1000$, $0.001 \leq y < 1$, $1 \leq \tilde{p} \leq 1000$.



line at the fixed ratio of $\tilde{p}/\Lambda \sim 0.75$.¹⁰ The depth of the valley is proportional to Λ^4 . Because E_{Cas} is the (\tilde{p}, y) 'flat-plane' integral of $\tilde{p}^3 F(\tilde{p}, y)$, the *volume* inside the valley is the quantity E_{Cas} . It is easy to see E_{Cas} is proportional to Λ^5 . This is consistent with (24). Importantly, (49) shows the *scaling* behaviour for large values of Λ and l . From a *close* numerical analysis of (\tilde{p}, y) -integral (49), we have confirmed (See App.C)

$$E_{Cas}(\Lambda, l) = \frac{2\pi^2}{(2\pi)^4} [-0.1249l\Lambda^5 - (1.41, 0.706, 0.353) \times 10^{-5} l\Lambda^5 \ln(l\Lambda)] \quad . \quad (52)$$

(Note: $0.125 = (1/8) \times (1/5) \times (4[even] + 1[odd])$.) This is the essentially-same result of Sec.2.¹¹

Finally we notice, from the Fig.2-4, the approximate form of $F(\tilde{p}, y)$ for the large Λ and l is given by

$$F(\tilde{p}, y) \approx -\frac{f}{2}\Lambda(1 - \frac{\tilde{p}}{\Lambda}) \quad , \quad f = 5 \quad , \quad (53)$$

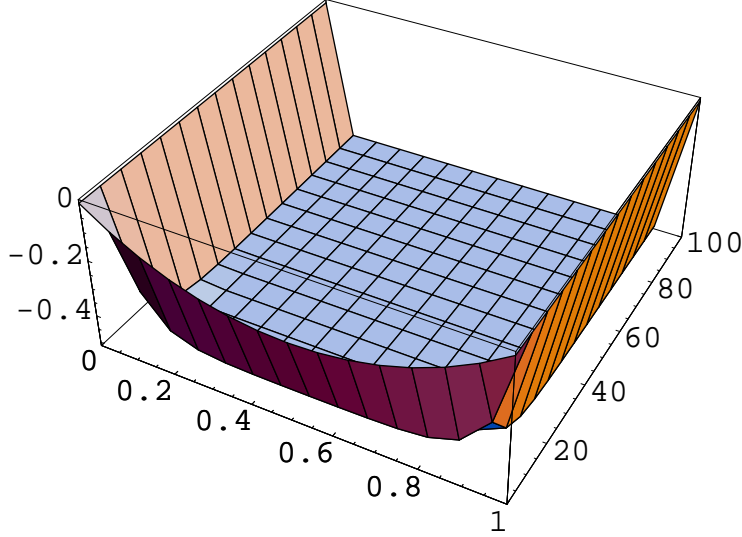
which does *not* depend on y and l .¹² f is the *degree of freedom*. From this result, we know,

¹⁰ The Valley-bottom line ('path') $\tilde{p} = \tilde{p}(y) \approx 0.75\Lambda$ corresponds to the solution of the minimal 'action' principle: $\delta S = 0$, $S \equiv (1/8\pi^2) \int d\tilde{p} \int dy \tilde{p}^3 F(\tilde{p}, y)$. This will be referred in Sec.7.

¹¹ Note that the result (24) of Sec.2 is obtained from the KK-expanded form, whereas that of this section (52) from the *closed* expression. The coincidence (Λ^5 proportionality) strongly shows the correctness of both evaluation. At the same time, the numerical result for the first term coefficient shows the the number of significant figures is 4. Although the second term contribution is tiny, its coefficient is not stable and its significant digits is 1 at most. The triplet data correspond to $l = 10, 20$ and 40 .

¹² Using the approximate form (53), E_{Cas} is estimated as $E_{Cas}(\Lambda, l) \times 8\pi^2 \approx \int_{1/l}^{\Lambda} d\tilde{p} \int_{1/\Lambda}^l dy \tilde{p}^3 (-5/2)(\Lambda - \tilde{p}) = -(1/8)l\Lambda^5(1 + O(\frac{1}{\Lambda}))$. This is consistent with (52).

Figure 5: Behaviour of the integrand of F^- , $IntgrdF^-(\tilde{k}, y; l)$ (54). $l = 1$, $\Lambda = 100$, $0 \leq y \leq l = 1$, $1 \leq \tilde{k} \leq \Lambda = 100$. The flat plane locates at the height -0.5.



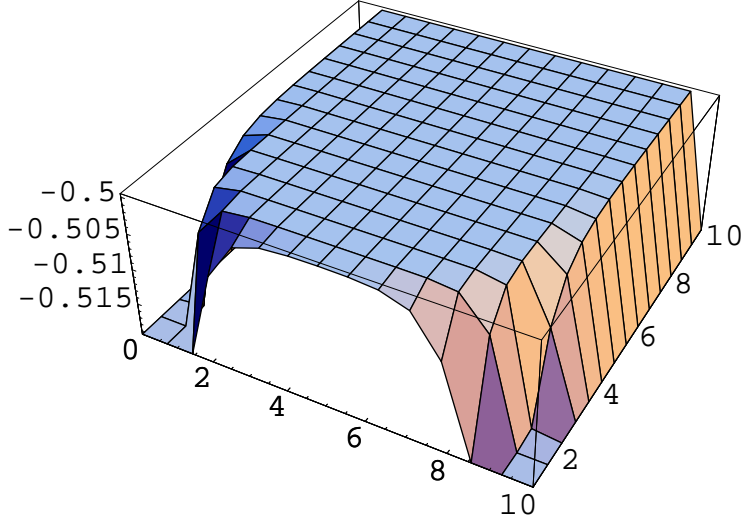
using the integral expression (47), the following *approximate* form about the integrand of F^\mp valid for the following wide-range (\tilde{k}, y) .

$$\begin{aligned} IntgrdF^-(\tilde{k}, y; l) &\equiv \frac{\cosh \tilde{k}(2y - l) - \cosh \tilde{k}l}{2 \sinh(\tilde{k}l)} \approx -\frac{1}{2} \quad , \\ IntgrdF^+(\tilde{k}, y; l) &\equiv \frac{-\cosh \tilde{k}(2y - l) - \cosh \tilde{k}l}{2 \sinh(\tilde{k}l)} \approx -\frac{1}{2} \quad , \\ (\tilde{k}, y) &\in \{(\tilde{k}, y) | \tilde{k}y \gg 1 \text{ and } \tilde{k}(l - y) \gg 1\} \end{aligned} \quad (54)$$

which can be analytically proved and is confirmed by graphically showing the above functions. See Fig.5 and Fig.6. The table-shape of the graphs implies the "Rayleigh-Jeans" dominance.¹³

¹³ The well-known radiation spectral formula (β the inverse temperature): $\langle E \rangle_{\nu, \beta} = h\nu/2 + h\nu/(e^{\beta h\nu} - 1)$ consists of two parts. The first one is the zero-point energy and the second is the Planck's distribution part. The low frequency region of the Planck's distribution formula: $h\nu/(e^{\beta h\nu} - 1) \approx 1/\beta$ (independent of ν), $h\nu \ll 1/\beta$, is called Rayleigh-Jeans's region. Note that the extra coordinate y or $l - y$, in the present 5D model, plays the role of the inverse temperature β .

Figure 6: Behaviour of the integrand of F^+ , $IntgrdF^+(\tilde{k}, y; l)$ (54). $l = 10$, $\Lambda = 10$, $0 \leq y \leq l = 10$, $1 \leq \tilde{k} \leq \Lambda = 10$. The flat plane locates at the height -0.5.

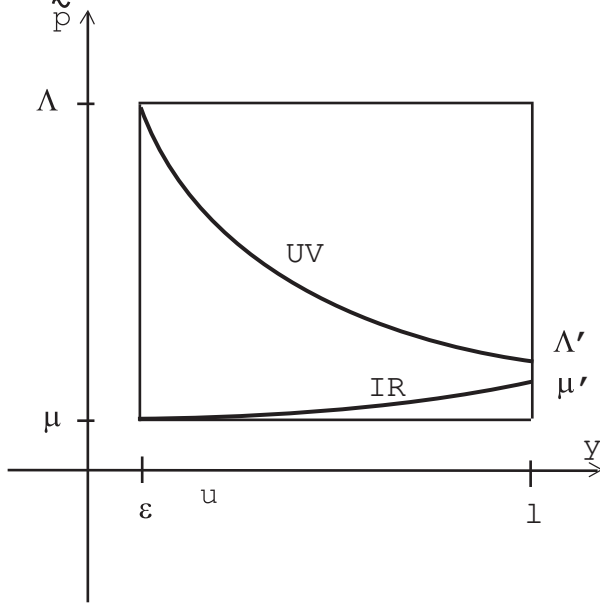


5 UV and IR Regularization Surfaces, Principle of Minimal Area and Renormalization Flow

We have confirmed the heat-kernel formulation is equivalent to the familiar KK-expansion approach. The advantage of the new approach is that the KK-expansion is replaced by the integral over the extra dimensional coordinate y and all expressions are written in the closed (not expanded) form. The Λ^5 -divergence shows the notorious problem of the higher dimensional theories. In spite of all efforts of the past literature, we have not succeeded in defining the higher-dimensional theories. (In this free theory case, the divergence is simple and the *finite* Casimir energy(force) can be read as shown in (25). In general, however, the divergences cause problems. The famous example is the divergent *cosmological constant* in the gravity-involving theories. [3]) We notice here we can solve the divergence problem if we find a way to *legitimately restrict the integral region in (\tilde{p}, y) -space*.

One proposal of this was presented by Randall and Schwartz[9]. They introduced the *position-dependent cut-off*, $\mu < \tilde{p} < 1/u$, $u \in [\epsilon, l]$, for the 4D-momentum integral in the "brane" located at $y = u$. (See Fig.1) The total integral region is the lower part of the hyperbolic curve $\tilde{p} = 1/y$. They succeeded in obtaining the *finite* β -function in the 5D warped vector model. We have confirmed that the value E_{Cas} of (49), when the Randall-Schwartz integral region (Fig.1) is taken, is proportional to Λ^4 . The close numerical analysis

Figure 7: Space of (\tilde{p}, y) for the integration (present proposal).



says (see App.C)

$$\begin{aligned}
 E_{Cas}^{RS} &= \frac{2\pi^2}{(2\pi)^4} \int_{1/l}^{\Lambda} dq \int_{1/\Lambda}^{1/q} dy q^3 F(q, y) = \frac{2\pi^2}{(2\pi)^4} \int_{1/\Lambda}^l du \int_{1/l}^{1/u} d\tilde{p} \tilde{p}^3 F(\tilde{p}, u) \\
 &= \frac{2\pi^2}{(2\pi)^4} [-8.93814 \times 10^{-2} \Lambda^4] \quad , \quad (55)
 \end{aligned}$$

which is *independent* of l .¹⁴ This shows the divergence situation is indeed improved compared with Λ^5 -divergence of (52).

Although they claim the holography (for the case of the warped geometry) is behind the procedure, the legitimacy of the restriction looks less obvious. We have proposed an alternate approach and given a legitimate explanation within the 5D QFT[10, 11, 12]. Here we closely examine the new regularization.

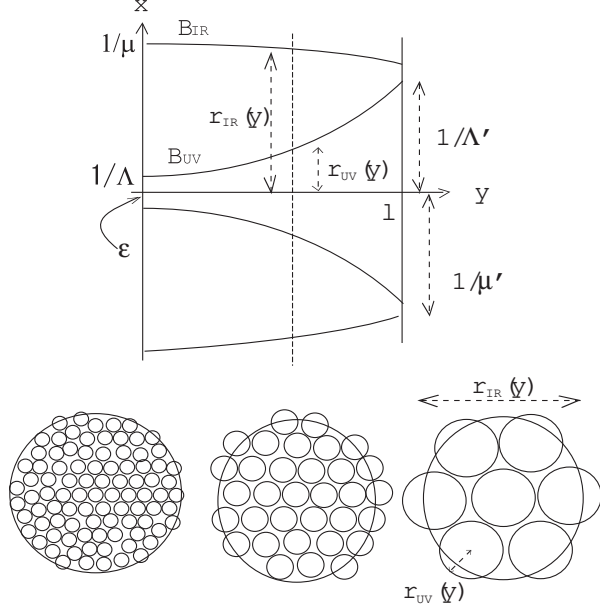
On the "3-brane" at $y = \epsilon$, we introduce the IR-cutoff μ and the UV-cutoff Λ ($\mu \ll \Lambda$). See Fig.7.

$$\mu \ll \Lambda \quad . \quad (56)$$

This is legitimate in the sense that we usually do this procedure in the 4D *renormalizable* theories. (Here we are considering those 5D theories that are renormalizable in 3-branes. Examples are 5D electromagnetism(the present model), 5D Φ^4 -theory, 5D Yang-Mills theory, e.t.c..) In the same reason, on the "3-brane" at $y = l$, we may have another set of IR

¹⁴ The result (55) is consistent with the approximate form of F (54). $(-5/2) \int_{1/l}^{\Lambda} dq \int_{1/\Lambda}^{1/q} dy q^3 (\Lambda - q) = -(1/12) \Lambda^4 (1 + O(1/(\Lambda l)^3))$. $0.0893 \approx 0.0833 \dots = 1/12$.

Figure 8: Regularization Surface B_{IR} and B_{UV} in the 5D coordinate space (x^μ, y) , Flow of Coarse Graining (Renormalization) and Sphere Lattice Regularization.



and UV-cutoffs, μ' and Λ' . We consider the case:

$$\mu' \leq \Lambda', \quad \Lambda' \ll \Lambda, \quad \mu \sim \mu' \quad . \quad (57)$$

This case will lead to allow us to introduce the *renormalization flow*. (See the later discussion.) We claim here, as for the "3-brane" located at each point y ($\epsilon < y < l$), the regularization parameters are determined by the *minimal area principle*.¹⁵ To explain it, we move to the 5D coordinate space (x^μ, y) . See Fig.8. The \tilde{p} -expression is replaced by $\sqrt{x_\mu x^\mu}$ -expression by the *reciprocal relation*.

$$\sqrt{x_\mu(y) x^\mu(y)} \equiv r(y) \quad \leftrightarrow \quad \frac{1}{\tilde{p}(y)} \quad . \quad (58)$$

The UV and IR cutoffs change their values along y -axis and the trajectories make *surfaces* in the 5D bulk space (x^μ, y) . We *require* the two surfaces do *not cross* for the purpose of the renormalization group interpretation (discussed later). We call them UV and IR regularization (or boundary) surfaces (B_{UV}, B_{IR}).

$$\begin{aligned} B_{UV} &: \quad \sqrt{(x^1)^2 + (x^2)^2 + (x^3)^2 + (x^4)^2} = r_{UV}(y) \quad , \quad \epsilon = \frac{1}{\Lambda} < y < l \quad , \\ B_{IR} &: \quad \sqrt{(x^1)^2 + (x^2)^2 + (x^3)^2 + (x^4)^2} = r_{IR}(y) \quad , \quad \epsilon = \frac{1}{\Lambda} < y < l \quad , \end{aligned} \quad (59)$$

¹⁵ We do *not* quantize the (bulk) geometry, but treat it as the *background*. The (bulk) geometry fixes the behavior of the *regularization* cut-off parameters in the field quantization. The geometry influences the "boundary" of the field-quantization procedure in this way.

The 5D volume region bounded by B_{UV} and B_{IR} is the integral region of the Casimir energy E_{Cas} . The forms of $r_{UV}(y)$ and $r_{IR}(y)$ can be determined by the *minimal area principle*.

$$\delta(\text{Surface Area}) = 0 \quad , \quad 3 - \frac{r \frac{d^2 r}{dy^2}}{1 + \left(\frac{dr}{dy}\right)^2} = 0 \quad , \quad 0 \leq y \leq l \quad (60)$$

In App.A, we present the classification of all solutions (paths) and the general analytic solution. In Fig.10, we show two result curves of (60) taking the boundary conditions ($r' \equiv dr/dy$) :

Fig.10: Fine Conf. goes to Coarse Conf. as y increases

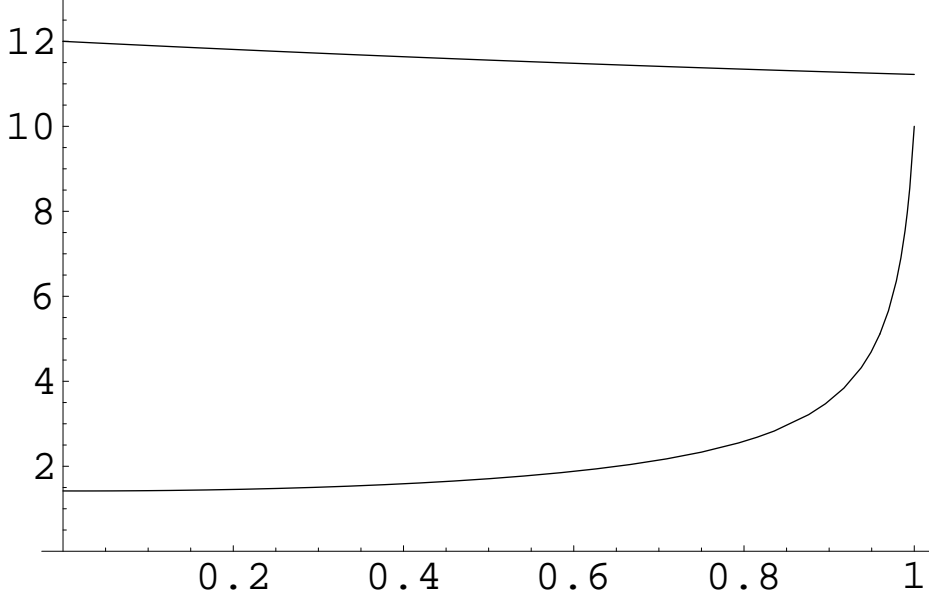
$$\begin{aligned} \text{IR-curve (upper):} \quad & r[0] = 12.0, r'[0] = -1.0 \quad [\text{simply-decreasing type}] \\ \text{UV-curve (lower):} \quad & r[1.0] = 10.0, r'[1.0] = 350.0 \quad [\text{simply-increasing type}] \end{aligned} \quad (61)$$

where the types of curves are specified on the basis of the classification of the minimal surface lines in App.A1. They show the renormalization flow shown in Fig.7 really occurs by the minimal area principle. In Fig.11 another set of minimal surface lines are given by taking another boundary conditions.

Fig.11: Coarse Conf. goes to Fine Conf. as y increases

$$\begin{aligned} \text{IR-curve (upper): } & r[0] = 4.6, r'[0] = -1.0 \text{ [simply-decreasing type]} \\ \text{UV-curve (lower): } & r[0] = 4.5, r'[0] = -22.0 \text{ [simply-decreasing type]} \end{aligned} \quad (62)$$

Figure 10: Numerical solution of (60). Vertical axis: r ; Horizontal axis $0 \leq y \leq l = 1$. IR-curve (upper): $r[0] = 12.0, r'[0] = -1.0$ [simply-decreasing type]; UV-curve (lower): $r[1.0] = 10.0, r'[1.0] = 350.0$ [simply-increasing type].



They show the opposite-direction flow of renormalization compared with Fig.10. (See the next paragraph for the renormalization flow interpretation.) These two examples imply the *boundary conditions* determine the property of the renormalization flow. ¹⁶

The present regularization scheme also gives the *renormalization group* interpretation to the change of physical quantities along the extra axis. See Fig.8. ¹⁷ In the "3-brane" located at y , the UV-cutoff is $r_{UV}(y)$ and the regularization surface is the sphere S^3 with the radius $r_{UV}(y)$. The IR-cutoff is $r_{IR}(y)$ and the regularization surface is the another sphere S^3 with the radius $r_{IR}(y)$. We can regard the regularization integral region as the *sphere lattice* of the following properties:

A unit lattice (cell) : the sphere S^3 with radius $r_{UV}(y)$ and its inside ,

Total lattice : the sphere S^3 with radius $r_{IR}(y)$ and its inside .

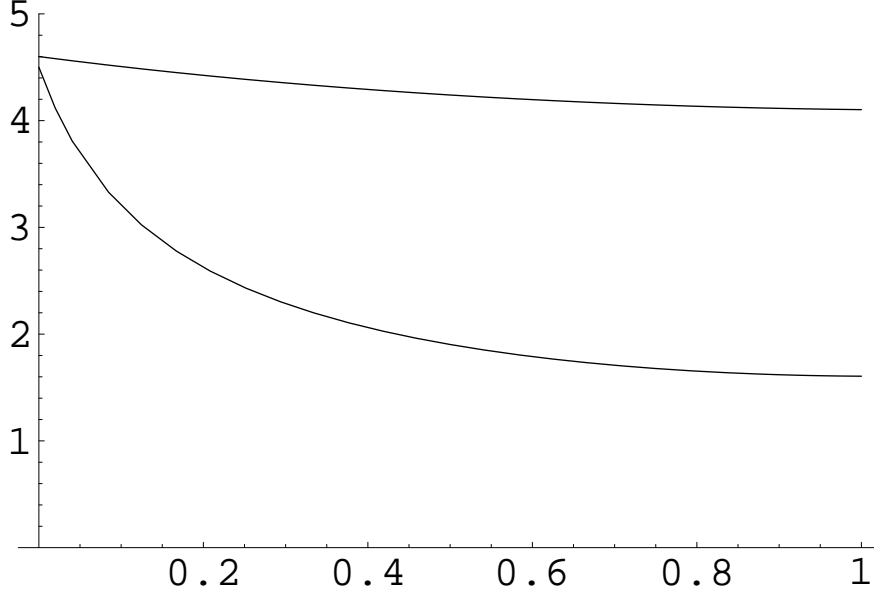
It is made of many cells above ,

$$\text{Total number of cells : } \text{const.} \times \left(\frac{r_{IR}(y)}{r_{UV}(y)} \right)^4 . \quad (63)$$

¹⁶ The minimal area equation (60) is the 2nd derivative differential equation and has the general solution. (See App.A) Hence, for given two initial conditions (for example, $r(y = \epsilon)$ and $dr/dy|_{y=\epsilon}$), there exists a unique analytic solution. The presented graphs are those with these initial conditions. Another choice of the initial conditions, $r(y = \epsilon)$ and $r(y = l)$, is possible. Generally the solution of the second derivative differential equation is fixed by two *boundary conditions*.

¹⁷ This part is contrasting with AdS/CFT approach where the renormalization flow comes from the Einstein equation of 5D supergravity.

Figure 11: Numerical solution of (60). Vertical axis: r ; Horizontal axis $0 \leq y \leq l = 1$. IR-curve (upper): $r[0] = 4.6, r'[0] = -1.0$ [simply-decreasing type]; UV-curve (lower): $r[0] = 4.5, r'[0] = -22.0$ [simply-decreasing type].



The total number of cells changes from $(\frac{\Lambda}{\mu})^4$ at $y = \epsilon$ to $(\frac{\Lambda'}{\mu'})^4$ at $y = l$. Along the y -axis, the number increase as

$$\left(\frac{r_{IR}(y)}{r_{UV}(y)} \right)^4 \equiv N(y) \quad . \quad (64)$$

For the "scale" change $y \rightarrow y + \Delta y$, N changes as

$$\Delta(\ln N) = 4 \frac{\partial}{\partial y} \left\{ \ln \left(\frac{r_{IR}(y)}{r_{UV}(y)} \right) \right\} \cdot \Delta y \quad . \quad (65)$$

When the system has some coupling $g(y)$, the renormalization group $\beta(g)$ -function (along the extra axis) is expressed as

$$\beta = \frac{\Delta(\ln g)}{\Delta(\ln N)} = \frac{1}{\Delta(\ln N)} \frac{\Delta g}{g} = \frac{1}{4} \frac{1}{\frac{\partial}{\partial y} \ln \left(\frac{r_{IR}(y)}{r_{UV}(y)} \right)} \frac{1}{g} \frac{\partial g}{\partial y} \quad , \quad (66)$$

where $g(y)$ is a renormalized coupling at y .¹⁸

We have confirmed that the minimal area principle determines the flow of the regularization surfaces. Among the numerical results, some curves are similar to the type proposed by Randall-Schwartz.

¹⁸ Here we consider interacting theories, such as 5D Yang-Mills theory and 5D Φ^4 theory, where the coupling $g(y)$ is the renormalized one in the '3-brane' at y .

6 Weight Function and Casimir Energy Evaluation

In the expression (47), the Casimir energy is written by the integral in the (\tilde{p}, y) -space over the range: $0 \leq y \leq l$, $0 \leq \tilde{p} \leq \infty$. In Sec.5, we see *the integral region should be properly restricted* because the cut-off region in the 4D world changes along the extra-axis obeying the bulk (flat) geometry (minimal area principle). In this section, we consider an alternate version.

We introduce, instead of restricting the integral region, a *weight function* $W(\tilde{p}, y)$ in the (\tilde{p}, y) -space for the purpose of suppressing UV and IR divergences of the Casimir Energy.

$$E_{Cas}^W(l) \equiv \int \frac{d^4 p}{(2\pi)^4} \int_0^l dy W(\tilde{p}, y) F(\tilde{p}, y) \quad , \quad F(\tilde{p}, y) \equiv F^-(\tilde{p}, y) + 4F^+(\tilde{p}, y) \quad ,$$

Examples of $W(\tilde{p}, y)$:

$$W(\tilde{p}, y) = \left\{ \begin{array}{ll} e^{-(1/2)l^2\tilde{p}^2 - (1/2)y^2/l^2} \equiv W_1(\tilde{p}, y) & \text{elliptic suppression} \\ e^{-(1/2)l^2\tilde{p}^2} \equiv W_{1b}(\tilde{p}, y) & \text{kinetic-energy suppression} \\ e^{-\tilde{p}y} \equiv W_2(\tilde{p}, y) & \text{hyperbolic suppression1} \\ e^{-(1/2)\tilde{p}^2 y^2} \equiv W_3(\tilde{p}, y) & \text{hyperbolic suppression2} \\ e^{-(1/2)l^4\tilde{p}^2/y^2} \equiv W_4(\tilde{p}, y) & \text{linear suppression} \\ e^{-l^3\tilde{p}/y^2} \equiv W_5(\tilde{p}, y) & \text{parabolic suppression1} \\ e^{-l^3\tilde{p}^2/y} \equiv W_6(\tilde{p}, y) & \text{parabolic suppression2} \\ e^{-(1/2)l^4\tilde{p}^4} \equiv W_7(\tilde{p}, y) & \text{higher-derivative suppression1} \\ e^{-(l^2/2)(\tilde{p}^2+1/y^2)} \equiv W_8(\tilde{p}, y) & \text{reciprocal suppression1} \\ e^{-(l^4/2)\tilde{p}^2(\tilde{p}^2+1/y^2)} \equiv W_{47}(\tilde{p}, y) & \text{higher-derivative suppression2} \\ e^{-(l^3/2)(\tilde{p}/y)(\tilde{p}+1/y)} \equiv W_{56}(\tilde{p}, y) & \text{reciprocal suppression2} \\ e^{-(l^4/2)(\tilde{p}^2+1/y^2)^2} \equiv W_{88}(\tilde{p}, y) & \text{higher-der reciprocal suppression} \\ e^{-(l^2/2)(\tilde{p}+1/y)^2} \equiv W_9(\tilde{p}, y) & \text{reciprocal suppression3} \end{array} \right. \quad (67)$$

where F^\mp are defined in (47).¹⁹ In the above, we list some examples expected for the weight function $W(\tilde{p}, y)$. W_2 and W_3 are regarded to correspond to the regularization taken by Randall-Schwartz. How to specify the form of W is the subject of the next section. We show the shape of the energy integrand $\tilde{p}^3 W(\tilde{p}, y) F(\tilde{p}, y)$ in Fig.12- 15. We notice the valley-bottom line $\tilde{p} \approx 0.75\Lambda$, which appeared in the un-weighted case (Fig.2-4), is replaced by new lines: $\tilde{p} \approx \text{const}$ (Fig.12 , W_1), $\tilde{p}y \approx \text{const}$ (Fig.13 , W_3), $\tilde{p} \approx \text{const} \times y$ (Fig.14 , W_4), $\tilde{p} \approx \text{const} \times \sqrt{y}$ (Fig.15 , W_6). They all are located away from the original Λ -effected line: $\tilde{p} \sim 0.75\Lambda$.

We can check the divergence (scaling) behaviour of E_{Cas}^W by numerically evaluate the

¹⁹ In the flat geometry, the periodicity parameter l is the unique scale parameter. We make all exponents in (67) dimensionless by use of l .

Figure 12: Behaviour of $\tilde{p}^3 W_1(\tilde{p}, y) F(\tilde{p}, y)$ (elliptic suppression). $\Lambda = 10$, $l = 1$. $1/\Lambda \leq y \leq 0.99999l$, $1/l \leq \tilde{p} \leq \Lambda$.

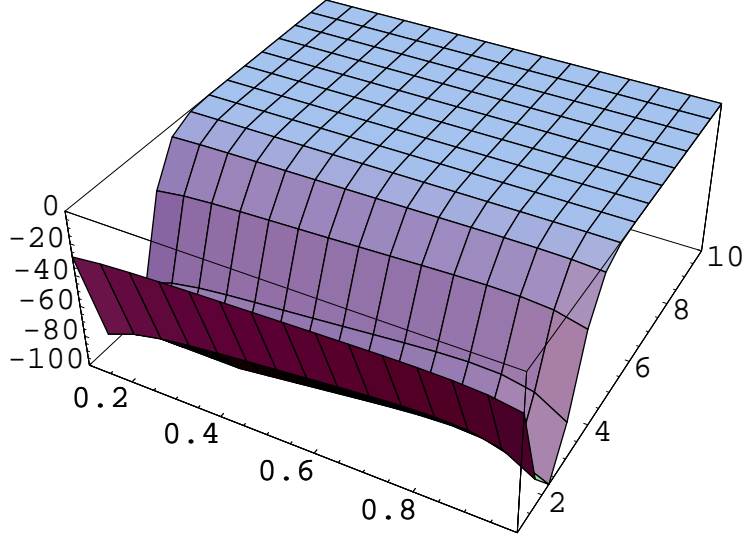


Figure 13: Behaviour of $\tilde{p}^3 W_3(\tilde{p}, y) F(\tilde{p}, y)$ (hyperbolic suppression2). $\Lambda = 10$, $l = 1$. $1/\Lambda \leq y \leq 0.99999l$, $1/l \leq \tilde{p} \leq \Lambda$.

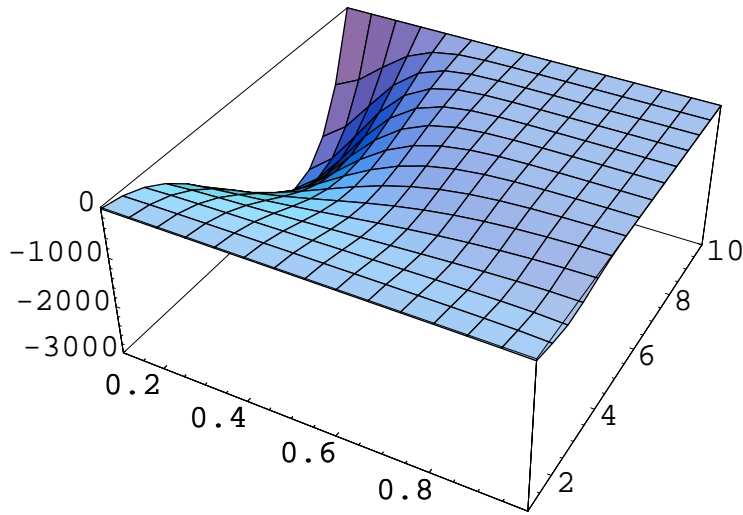


Figure 14: Behaviour of $\tilde{p}^3 W_4(\tilde{p}, y) F(\tilde{p}, y)$ (linear suppression). $\Lambda = 10$, $l = 0.5$. $1/\Lambda \leq y \leq 0.99999l$, $1/l \leq \tilde{p} \leq \Lambda$.

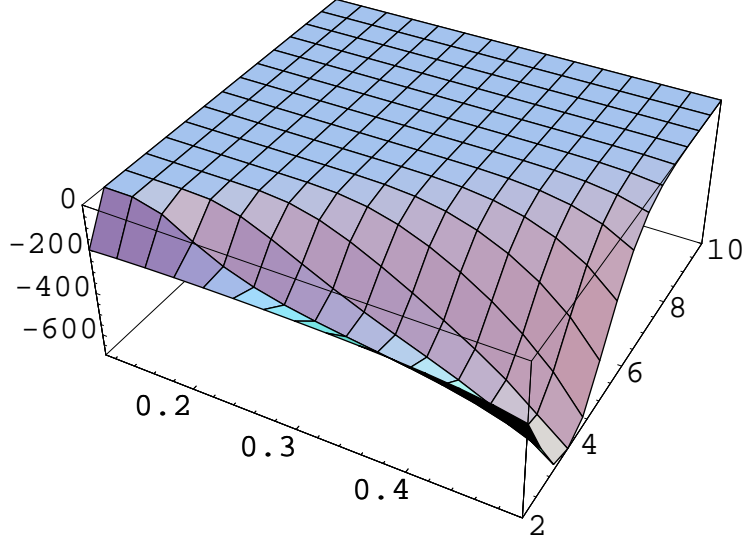
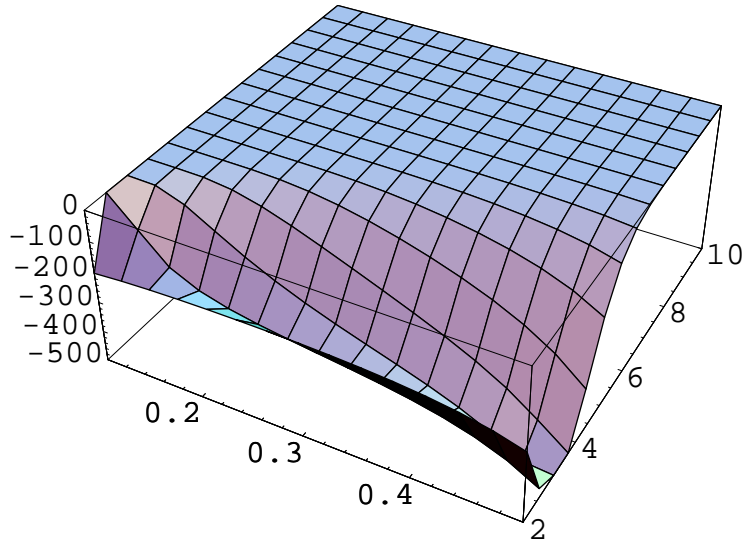


Figure 15: Behaviour of $\tilde{p}^3 W_6(\tilde{p}, y) F(\tilde{p}, y)$ (parabolic suppression2). $\Lambda = 10$, $l = 0.5$. $1.001/\Lambda \leq y \leq 0.99999l$, $1/l \leq \tilde{p} \leq \Lambda$. The contour of this graph is given later in Fig.20.



(\tilde{p}, y) -integral (67) for the rectangle region of Fig.1. ²⁰

$$E_{Cas}^W \times 2^3 \pi^2 = \left\{ \begin{array}{ll} -(3.892, 3.894, 3.894) \frac{\Lambda}{l^3} + (-0.221, 1.70, 1.76) \times 10^{-4} \frac{\Lambda \ln(l\Lambda)}{l^3} & \text{for } W_1 \\ -(4.554, 4.554, 4.553) \frac{\Lambda}{l^3} + (4.36, 4.44, 3.34) \times 10^{-4} \frac{\Lambda \ln(l\Lambda)}{l^3} & \text{for } W_{1b} \\ -(0.120784, 0.120788, 0.120789) \Lambda^4 - (49.4, 5.58, 3.20) \times 10^{-8} \Lambda^4 \ln(l\Lambda) & \text{for } W_2 \\ -(7.0999, 6.14611, 6.14610) \times 10^{-2} \Lambda^4 + (102.2, 1.3086416, 1.3086413) \times 10^{-5} \Lambda^4 \ln(l\Lambda) & \text{for } W_3 \\ -(0.820, 0.814, 0.811) \frac{\Lambda}{l^3} + (1.47, 0.847, 0.478) \times 10^{-3} \frac{\Lambda \ln(l\Lambda)}{l^3} & \text{for } W_4 \\ -(1.62, 1.61, 1.60) \frac{\Lambda}{l^3} + (3.87, 2.30, 1.33) \times 10^{-3} \frac{\Lambda \ln(l\Lambda)}{l^3} & \text{for } W_5 \\ -(0.2478, 0.2466, 0.2458) \frac{\Lambda}{l^3} + (3.12, 1.79, 1.01) \times 10^{-4} \frac{\Lambda \ln(l\Lambda)}{l^3} & \text{for } W_6 \\ -(0.761, 0.760, 0.759) \frac{\Lambda}{l^3} + (2.58, 1.67, 1.02) \times 10^{-4} \frac{\Lambda \ln(l\Lambda)}{l^3} & \text{for } W_7 \\ -(0.957, 0.955, 0.953) \frac{\Lambda}{l^3} + (7.40, 4.39, 2.54) \times 10^{-4} \frac{\Lambda \ln(l\Lambda)}{l^3} & \text{for } W_8 \\ -(0.0993, 0.0992, 0.0992) \frac{\Lambda}{l^3} + (2.13, 2.07, 1.95) \times 10^{-4} \frac{\Lambda \ln(l\Lambda)}{l^3} & \text{for } W_{47} \\ -(0.342, 0.340, 0.339) \frac{\Lambda}{l^3} + (5.79, 3.34, 1.89) \times 10^{-4} \frac{\Lambda \ln(l\Lambda)}{l^3} & \text{for } W_{56} \\ -(1.307, 1.306, 1.303) \times 10^{-2} \frac{\Lambda}{l^3} + (6.02, 5.84, 5.52) \times 10^{-5} \frac{\Lambda \ln(l\Lambda)}{l^3} & \text{for } W_{88} \\ -(9.95, 9.89, 9.86) \times 10^{-2} \frac{\Lambda}{l^3} + (14.72, 8.48, 4.80) \times 10^{-5} \frac{\Lambda \ln(l\Lambda)}{l^3} & \text{for } W_9 \end{array} \right. \quad (68)$$

The above fitting is obtained by taking the data for the range: $l = (10, 20, 40)$, $\Lambda = 10 \sim 10^3$. The round-bracketed triplet data, corresponding to 3 values of l , should be the same if the scaling region is properly examined. The small fluctuation in the last digit number tells us the significant figures. The leading terms are firmly obtained, and the significant digit number ≥ 3 . Whereas the log-terms are obtained very poorly, and the significant digit number is 1 at best. ²¹ The suppression behaviors of W_2 and W_3 are consistent with (55) by Randall-Schwartz. ²² The hyperbolic suppressions, however, are insufficient for the renormalizability. The desired cases are others. They give, after normalizing the factor Λl , *only the log-divergence*.

$$E_{Cas}^W / \Lambda l = -\frac{\alpha}{l^4} (1 - 4c \ln(l\Lambda)) \quad (69)$$

where α can be read from (68) depending on the choice of W . (For the 5D EM (24), $\alpha = 5 \times 3\zeta(5)/(4 \times 8\pi^2) \approx 3.86/8\pi^2$.) As for c , we expect it reaches a fixed value as l increases furthermore. Although the present approach leaves the weight function $W(\tilde{p}, y)$ unspecified, and the numerical results involve some ambiguity, we may say $\alpha \times 2^3 \pi^2$ is a positive number and the order of $O(10^{-2}) \sim O(1)$, c is a positive number of the order of $O(10^{-3})$.

At present, we cannot discriminate which weight is the right one. Here we list characteristic features (advantageous(Yes) or disadvantageous(No), independent (I) or dependent(D), singular(S) or regular(R)) for each weight from the following points.

²⁰ See App.C for the explanation of the numerical derivation.

²¹ The unstableness of data does not appear in the warped case[12].

²² In particular, W_2 is more similar to (55) in that the log-term vanishes in the present numerical precision.

- point 1** As $l \rightarrow 0$, $W(\tilde{p}, y) \rightarrow 1$. (This is favoured because the continuity to the ordinary 4D field-quantization is guaranteed by this property.)
- point 2** The path (bottom line of the valley) is independent(I) of the scale l or dependent(D) on it.
- point 3** Regular(R) or singular(S) at $y = 0$.
- point 4** Symmetric for $l\tilde{p} \leftrightarrow y/l$.
- point 5** Symmetric for $\tilde{p} \leftrightarrow 1/y$. (Reciprocal symmetry)
- point 6** Casimir energy is finite.
- point 7** Value of $\alpha \times 8\pi^2$.
- point 8** Under the Z_2 -parity: $y \leftrightarrow -y$, $W(\tilde{p}, y)$ is even (E), odd (O) or none (N).

type	W_1	W_{1b}	W_2	W_3	W_4	W_5	W_6	W_7	W_8	W_{47}	W_{56}	W_{88}	W_9
p. 1	N	Y	N	N	Y	Y	Y	Y	Y	Y	Y	Y	Y
p. 2	D	D	I	I	D	D	D	D	D	D	D	D	D
p. 3	R	R	R	R	S	S	S	R	S	S	S	S	S
p. 4	Y	$/$	Y	Y	$/$	N	N	$/$	$/$	N	$/$	$/$	$/$
p. 5	$/$	$/$	$/$	$/$	Y	N	N	$/$	Y	N	Y	Y	Y
p. 6	Y	Y	N	N	Y	Y	Y	Y	Y	Y	Y	Y	Y
p. 7	3.9	4.6	$/$	$/$	0.81	1.6	0.25	0.76	0.95	0.099	0.34	0.013	0.099
p. 8	E	E	O	E	E	E	O	E	E	E	N	E	N

So far as the legitimate reason of the introduction of $W(\tilde{p}, y)$ is not clear, we should regard this procedure as a *regularization* to define the higher dimensional theories. We give a definition of $W(\tilde{p}, y)$ and a legitimate explanation in the next section. It should be done, in principle, in a consistent way with the bulk geometry and the gauge principle.

7 Definition of Weight Function and Dominant Path

In the previous section, the weight function $W(\tilde{p}, y)$ is introduced as some trial functions to suppress the UV and IR divergences. In this section, we define (or specify) the weight function $W(\tilde{p}, y)$ properly and give a *legitimate reason* for the introduction of W .

First of all, the requirement of controlling the Λ^5 -divergence of Sec.4 makes us introduce some "damping" function $W(\tilde{p}, y)$ as in (67). Casimir energy is obtained by integrating out $W(\tilde{p}, y)F(\tilde{p}, y)$ over all 5D space region. Among all configurations involving the integral, there exists the dominant configuration which contributes to the integral most dominantly. The present claim is that the dominant configuration should be fixed by the 5D geometry,

that is, the 5D flat space(-time) with the periodic boundary condition and Z_2 -symmetry. In the integral (67), the *dominant path* $\tilde{p} = \tilde{p}_W(y)$ is characterized by the differential equation obtained by the variation method: $\tilde{p} \rightarrow \tilde{p} + \delta\tilde{p}$, $y \rightarrow y + \delta y$ in the (\tilde{p}, y) -integral expression (67).²³ Here we *require*, based on the present claim, the dominant path $\tilde{p}_W(y)$ coincides with the curve $r = r_g(y)$ (or its momentum counterpart $\tilde{p}_g(y)$, (93)) which is determined by the minimal area condition (60). Note that the minimal area curve $r = r_g(y)$ is defined by the 5D geometry.²⁴

To explain the previous paragraph using only the coordinate $(r = \sqrt{x^a x^a}, y)$, we move to the coordinate expression by the partially-Fourier-transformation. The Casimir energy (67) is re-expressed as

$$\begin{aligned} \hat{F}(r(x), y) &= \int \frac{d^4 p}{(2\pi)^4} e^{ipx} F(\tilde{p}, y) \quad , \quad \hat{W}(r(x), y) = \int \frac{d^4 p}{(2\pi)^4} e^{ipx} W(\tilde{p}, y) \quad , \\ r(x) &\equiv \sqrt{(x^1)^2 + (x^2)^2 + (x^3)^2 + (x^4)^2} \quad , \\ E_{Cas}^W(l) &= \int d^4 x \int_0^l dy \hat{W}(r(x), y) \hat{F}(r(x), y) = \\ &2\pi^2 \int_0^l dy \int_0^\infty dr \exp\{3 \ln r + \ln \hat{W}(r, y) + \ln \hat{F}(r, y)\} \quad . \end{aligned} \quad (70)$$

The un-weighted case is $\hat{W}(r(x), y) = \delta^4(x)$, $W(\tilde{p}, y) = 1$. The dominant contribution (path) $r = r_W(y)$ to E_{Cas}^W is given by the *minimal 'action' principle*, that is, applying the steepest-descend method to (70).

$$\frac{dr}{dy} = \frac{-\frac{1}{\hat{W}} \frac{\partial \hat{W}}{\partial y} - \frac{1}{\hat{F}} \frac{\partial \hat{F}}{\partial y}}{\frac{3}{r} + \frac{1}{\hat{W}} \frac{\partial \hat{W}}{\partial r} + \frac{1}{\hat{F}} \frac{\partial \hat{F}}{\partial r}} \equiv \hat{\mathcal{V}}_1(\hat{W}, \partial_r \hat{W}, \partial_y \hat{W}; r, y) \quad . \quad (71)$$

(The valley-bottom lines appeared in Fig.12-15 are regarded as the dominant paths.)
Using the above result, we can obtain $d^2 r / dy^2$.

$$\begin{aligned} \hat{\mathcal{W}}_y &\equiv \frac{1}{\hat{W}} \frac{\partial \hat{W}}{\partial y} + \frac{1}{\hat{F}} \frac{\partial \hat{F}}{\partial y} \quad , \quad \hat{\mathcal{W}}_r \equiv \frac{1}{\hat{W}} \frac{\partial \hat{W}}{\partial r} + \frac{1}{\hat{F}} \frac{\partial \hat{F}}{\partial r} \quad , \\ \frac{d^2 r}{dy^2} &= -\frac{\partial_y \hat{\mathcal{W}}_y}{3r^{-1} + \hat{\mathcal{W}}_r} + \frac{\hat{\mathcal{W}}_y(\partial_r \hat{\mathcal{W}}_y + \partial_y \hat{\mathcal{W}}_r)}{(3r^{-1} + \hat{\mathcal{W}}_r)^2} - \frac{\hat{\mathcal{W}}_y^2(-3r^{-2} + \partial_r \hat{\mathcal{W}}_r)}{(3r^{-1} + \hat{\mathcal{W}}_r)^3} \\ &\equiv \hat{\mathcal{V}}_2(\hat{W}, \partial_r \hat{W}, \partial_y \hat{W}, \partial_r^2 \hat{W}, \partial_y \partial_r \hat{W}, \partial_y^2 \hat{W}; r, y) \quad . \end{aligned} \quad (72)$$

²³ When $W(\tilde{p}, y) = 1$, the dominant path appears as $\tilde{p}(y) \approx 0.75\Lambda(\text{ind. of } y)$ in Fig.2-4. This path, however, is "artificially" created by the UV-cutoff. It is irrelevant to the 5D geometry. The differential equation of $\tilde{p}_W(y)$ is obtained in (95).

²⁴ In Sec.5, we have required the minimal area condition on the UV and IR regularization surfaces(boundary configuration), whereas, in this section we require it on the dominant configuration(to E_{Cas}) in the (\tilde{p}, y) or (r, y) -integral. In other words, we have *fixed* the 'dominant' configuration(path) , around which the small ("quantum") fluctuation may occur, by taking the minimal surface curve.

We *require* here that the path $r = r_W(y)$ of (71), which is defined in the $\hat{W}(r, y)$ -dependent way, coincides with the minimal surface curve $r_g(y)$ (60), which is defined independently of $\hat{W}(r, y)$. Hence $\hat{W}(r, y)$ is defined by, by inserting (71) and (72) in (60),

$$\hat{\mathcal{V}}_2(\hat{W}, \partial_r \hat{W}, \partial_y \hat{W}, \partial_r^2 \hat{W}, \partial_y \partial_r \hat{W}, \partial_y^2 \hat{W}; r, y) - \frac{3}{r} \{ \hat{\mathcal{V}}_1(\hat{W}, \partial_r \hat{W}, \partial_y \hat{W}; r, y) \}^2 - \frac{3}{r} = 0 \quad . \quad (73)$$

We call this equation "W-defining equation". It defines the weight function $\hat{W}(r, y)$ in terms of the bulk metric (geometry) and the model information \hat{F} . (Note: \hat{F} is given by (49).) In App.B.2, we treat the W-defining equation in $(\tilde{p} = \sqrt{p^a p^a}, y)$ variables. Besides, how much the trial weight functions satisfy the above definition is numerically examined.

The scaling of the renormalized coupling $g(y)$ is given by

$$\beta = -\frac{1}{4} \frac{1}{\frac{\partial}{\partial y} \ln r(y)} \frac{1}{g} \frac{\partial g}{\partial y} \quad , \quad (74)$$

where $g(y)$ is a renormalized coupling at y . In the above derivation, the formula (66) is used for the case : $\frac{\partial}{\partial y} r_{IR}(y) = 0$, $r_{UV}(y) = r(y)$.

8 Discussion and Conclusion

Let us suppose that we have found the right weight function and the divergences are successfully suppressed logarithmically. The Casimir energy (24) is replaced by

$$8\pi^2 E_{Cas} = -\frac{3}{4} \frac{\zeta(5)}{l^4} (1 - 4c \ln(l\Lambda)) = -\frac{3}{4} \frac{\zeta(5)}{l'^4} \quad , \quad (75)$$

where c is some constant(See (69)). It shows the periodicity parameter(or the compactification size) l changes as the renormalization scale changes. *The parameter l suffers from the renormalization effect.* It shows the field's *interaction with the boundaries*. The above relation is *exact* because the present system is the *free* theory, and the heat-kernel (1-loop) approach can be regarded as a *complete (non-perturbative)* quantum treatment[23]. Note that, in the familiar 4D renormalizable interacting theories, the 1-loop effect is proportional to (coupling)². In the present case, however, c is a *pure number*. When c is regarded small $c \ll 1$, we can approximate as ²⁵

$$l' \approx l(1 + c \ln(l\Lambda)) \quad , \quad (76)$$

The scaling behaviour of l is given by

$$\beta_l \text{ (}\beta\text{-function)} = \frac{\partial}{\partial(\ln \Lambda)} \ln \frac{l'}{l} = c \quad . \quad (77)$$

²⁵ From the results of (68), $c \sim O(10^{-3})$.

When $c > 0$, the compactification size l *grows* (*shrinks*) as the cut-off scale Λ *increases* (*decreases*), while when $c < 0$, l *shrinks* (*grows*) as the cut-off scale Λ *increases* (*decreases*). The former case is expected. When $c = 0$, it means the size l has no quantum effect.²⁶

The present 5D geometry is flat. The interesting application is the warped case. The analysis is under way. Partial interesting results are obtained[12]. More or less, the arguments go in the similar way to the flat case except that the periodic and hyperbolic functions are replaced by the Bessel and modified Bessel ones. The essential difference is that one additional massive parameter, the 5D AdS curvature, comes into the expressions. E_{Cas} is expressed by the massive parameter in addition to l and Λ .

In the present standpoint, the space-time geometric field G_{MN} is regarded as a background one. It is *not* quantized. As for other bulk fields, we assume they are renormalizable in the 3-brane. The role of the geometry appears in *requiring* the dominant 'path', determined by the (EM) field quantization, coincides with the geometrically-determined 'path' (*minimal area principle*). Practically W plays the role of suppressing the integral by weighting the original integrand. Although we have already stated the definition of W in Sec.7 and App.B, it is important to know the true meaning of W . In the next paragraph, we argue one possible interpretation.

In order to most naturally accomplish the above requirement, we can go to a new step. That is, we *propose* to *replace* the 5D space integral, in (70), by the following *path-integral*. Namely we *newly define* the Casimir energy in the higher-dimensional theory as follows.

$$\begin{aligned}\mathcal{E}_{Cas}(l, \Lambda) &\equiv \int_{1/\Lambda}^l d\rho \int_{\tilde{p}(0)=\tilde{p}(l)=1/\rho} \prod_{a,y} \mathcal{D}p^a(y) F(\tilde{p}, y) \exp \left[-\frac{1}{2\alpha'} \int_0^l \frac{1}{\tilde{p}^3} \sqrt{\frac{\tilde{p}'^2}{\tilde{p}^4} + 1} dy \right] \\ &= \int_{1/\Lambda}^l d\rho \int_{r(0)=r(l)=\rho} \prod_{a,y} \mathcal{D}x^a(y) F\left(\frac{1}{r}, y\right) \exp \left[-\frac{1}{2\alpha'} \int_0^l \sqrt{r'^2 + 1} r^3 dy \right], \quad (78)\end{aligned}$$

where the limit $\Lambda \rightarrow \infty$ is taken and the surface (string) tension parameter $T = 1/2\alpha'$ is introduced (note: the dimension of α' is [length]⁴). $F(\tilde{p}, y)$ or $F(1/r, y)$ is the energy density operator induced from the quantization of 5D EM fields at (47). The weight factor comes from the *area* suppression: $\exp(-\text{Area}/2\alpha') = \exp[-(1/2\alpha') \int \sqrt{\det g_{ab}} d^4x]$. In the above expression, we have followed the path-integral formulation of the density matrix (see Feynman's text[27]). The above definition clearly shows the 4D space-coordinates x^a or the 4D momentum-coordinates p^a are *statistically quantized* with the Euclidean time y and the "area Hamiltonian" $H = \int \sqrt{\det g_{ab}} d^4x$.²⁷ This reminds us of the *space-time uncertainty principle* [28] introduced in the development of the string theory. The 5D quantum field theory leads to some *quantum statistical* system of the 4D coordinates $\{x^a(y)\}$ with the inverse temperature parameter y . In this view, the treatment of Sec.6 and

²⁶ In the unified theories based on the string theory, l is called *moduli parameter* and is given by the vacuum expectation value of the dilaton field. How to fix the parameter is the moduli stabilization problem.

²⁷ The possibility of the quantum feature of the 5D coordinate/momenta was pointed out in Ref.[26] where the idea of the phase space (y, \tilde{p}) was presented in relation to the divergence problem of the "deformed" propagator in a 5D bulk-boundary theory.

Sec.7 is an *effective* action approach. We expect the direct evaluation of (78), numerically or analytically, leads to the similar result.

In the present analysis, from the beginning, the extra space is treated differently from the 4D real space(-time). It is regarded as the part which provides the axis for *scale* change. The change of renormalization group is determined by the *minimal area condition*. In order to extend the quantum field theory, without the divergence problem, the extra space should play a role to *suppress* the singular behaviour. Although the geometry is treated as a background, the final outcome looks to demand some type of quantization among the 4D coordinates (or momenta) as explained in the previous paragraph. The necessity of the weight function $W(\tilde{p}, y)$ in (67) can be interpreted as that we must take the well-defined space(-time) measure $d^4p dy W(\tilde{p}, y)$, instead of $d^4p dy$ ((47) or (49)) in summing over 5D space(-time).

We have focused only on the vacuum energy. We must, of course, examine other physical quantities such as S-matrix amplitude in the interacting theories.

The present proposal should be compared with the string theory. We do not directly treat the string propagation. We start with quantizing the higher dimensional field theory in the standard way of QFT. We *require* the dominant configuration, the path $r = r_W(y)$, to be equal to the solution of the minimal area line $r_g(y)$ by introducing the weight function $W(\tilde{p}, y)$. The bulk geometry takes part in the "coordinates quantization" by *fixing the central configuration* in this way. The closed-string-like configuration comes into this formalism through the *minimal area principle*. The field theories, which are applicable to this formalism, are limited to those that are renormalizable on the 3-brane, such as 5D Φ^4 -theory, 5D YM theory, 5D QED. But the advantageous points of this approach is that it is based on the QFT, hence we can expect various phenomenology application. We stress the practical importance.

We have pointed out a possibility to quantize the higher dimensional field theories within QFT.

9 Appendix A: Minimal Surface Curve in 5D Flat Space

We analytically examine the minimal area equation (60) in the 5D flat geometry.

$$3 - \frac{r\ddot{r}}{1 + \dot{r}^2} = 0 \quad , \quad 0 \leq y \leq l \quad , \quad (79)$$

where $\dot{r} = dr/dy$ and $\ddot{r} = d^2r/dy^2$.

9.1 A.1 Classification of Minimal Surface Curves

Before solving the equation, we classify all solutions using the differential equation above. This is useful in drawing minimal surface curves and in confirming the non-crossing of curves. (The requirement comes from the renormalization-group flow interpretation of the curves. See a few sentences above (59).)

In terms of $u \equiv 1/r^2$, the above one can be expressed as

$$u(y) \equiv \frac{1}{r(y)^2} = \frac{1}{x^a x^a} > 0 \quad ,$$

$$\text{flat limit}(\omega = 0) \quad : \quad \ddot{u} = -6u^2 \leq 0 \quad , \quad 0 \leq y \leq l \quad . \quad (80)$$

From this equation we know an important *inequality relation*:

$$\dot{u}|_{y=l} - \dot{u}|_{y=0} = -6 \int_0^l u^2 dy < 0 \quad . \quad (81)$$

The inequality $\ddot{u} \leq 0$ in (80) implies $u(y)$ is convex upwards.

Making use of the above relation, we can classify all solutions (paths) as follows.

(i) $\dot{u}(y=0) > 0$

(ia) $\dot{u}(l) > 0$

In this case $\dot{u}(y) > 0$ for $0 \leq y \leq l$. $u(y)$ is simply increasing ($r(y)$ is simply decreasing),

Fig.16

(ib) $\dot{u}(l) < 0$

(ib α) $u(0) < u(l)$ Fig.17

(ib β) $u(0) > u(l)$ Fig.18

(ii) $\dot{u}(y=0) < 0$

$u(y)$ is simply decreasing ($r(y)$ is simply increasing), Fig.19

Although numerical solutions are displayed in Fig.16-19, the general analytic solution is obtained in App.A.2. We have confirmed the high-precision equality between the numerical curves and the analytical ones.

Figure 16: Geodesic Curve $r(y)$ of (79) by Runge-Kutta method. Type (ia) Simply-Decreasing. $r(0) = 4.472, \dot{r}(0) = -22.36$

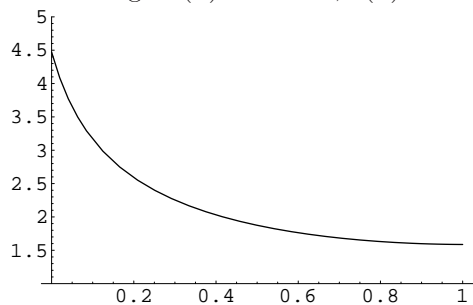


Figure 17: Geodesic Curve $r(y)$ of (79) by Runge-Kutta method. Type (ib α). $r(0) = 2.236, \dot{r}(0) = -5.590$

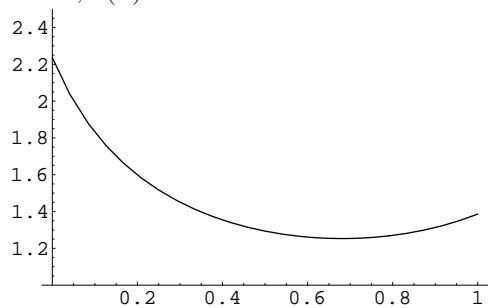


Figure 18: Geodesic Curve $r(y)$ of (79) by Runge-Kutta method. Type (ib β). $r(0) = 1.4142, \dot{r}(0) = -1.4142$

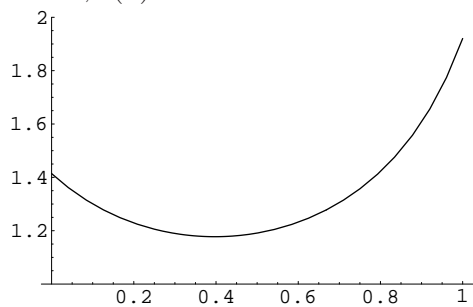
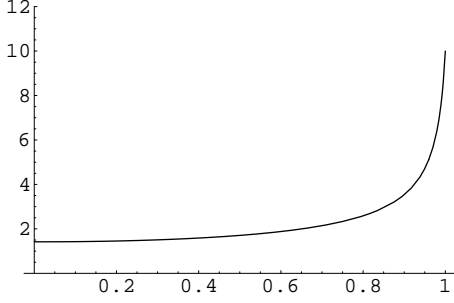


Figure 19: Geodesic Curve $r(y)$ of (79) by Runge-Kutta method. Type (ii) Simply-Increasing. $r(1.0) = 10.0, \dot{r}(1.0) = 350.0$



9.2 A.2 General Analytic Solution of Minimal Surface Curve (60,79,80)

We solve the differential equation (60,79,80) which is the minimal surface trajectory of the 5D *flat* geometry. The first integral is given by

$$\begin{aligned} \frac{d}{dy} \left(\frac{1}{2} \dot{u}^2 + 2u^3 \right) &= 0 \quad , \\ \frac{1}{2} \dot{u}^2 + 2u^3 &= 2C \quad , \quad C(>0) : \text{an integral constant} \\ \dot{u} = \frac{du}{dy} &= \pm 2\sqrt{C - u^3} \quad , \quad 0 < u \leq \sqrt[3]{C} \quad . \end{aligned} \quad (82)$$

We see the present classical system is equivalent to one particle mechanics with the potential $V = 2u^3$. The second integral is obtained as follows.

$$\int \frac{du}{\sqrt{C - u^3}} = \pm 2 \int dy = \pm 2y + C' \quad , \quad C' : \text{another integral constant} \quad . \quad (83)$$

The LHS of the above equation can be integrated as

$$\begin{aligned} v &\equiv \frac{u}{\sqrt[3]{C}} \quad , \quad 0 < v \leq 1 \quad , \\ \int \frac{du}{\sqrt{C - u^3}} &= \frac{\sqrt[3]{C}}{\sqrt{C}} \int \frac{dv}{\sqrt{1 - v^3}} = -\frac{C^{-1/6}}{\sqrt[4]{3}} F(\cos^{-1} \frac{\sqrt{3} - 1 + v}{\sqrt{3} + 1 - v}, \frac{\sqrt{3} + 1}{2\sqrt{2}}) \quad , \end{aligned} \quad (84)$$

where $F(\varphi, k)$ is the *elliptic integral of the first kind* and the following integral formula is used.

$$\begin{aligned} \int_v^1 \frac{dx}{\sqrt{1 - x^3}} &= \frac{1}{\sqrt[4]{3}} F(\cos^{-1} \frac{\sqrt{3} - 1 + v}{\sqrt{3} + 1 - v}, \frac{\sqrt{3} + 1}{2\sqrt{2}}) \quad , \quad 0 < \frac{\sqrt{3} - 1 + v}{\sqrt{3} + 1 - v} \leq 1 \quad , \\ F(\varphi, k) &= \int_0^\varphi \frac{d\theta}{\sqrt{1 - k^2 \sin^2 \theta}} = \int_0^{z_1} \frac{dz}{\sqrt{(1 - z^2)(1 - k^2 z^2)}} \equiv \tilde{F}(z_1, k) \quad , \\ 0 &\leq k \leq 1 \quad , \quad -\frac{\pi}{2} < \varphi < \frac{\pi}{2} \quad , \quad z_1 \equiv \sin \varphi = \text{sn}(\tilde{F}, k) \quad , \end{aligned} \quad (85)$$

where $\text{sn}(\tilde{F}, k)$ is defined by the inverse function of $\tilde{F}(z_1, k)$ and is called *Jacobi's elliptic function*. It has the period $4K(k) \equiv 4F(\frac{\pi}{2}, k)$. Hence,

$$\begin{aligned} z_1 = \sin \varphi &= \pm \sqrt{1 - \cos^2 \varphi} = \pm \{(1 - \cos \varphi)(1 + \cos \varphi)\}^{1/2} \\ &= \pm \frac{2\sqrt[4]{3}\sqrt{1-v}}{\sqrt{3+1-v}} = \text{sn}(-\sqrt[4]{3}C^{1/6}(\pm 2y + C'), \frac{\sqrt{3}+1}{2\sqrt{2}}) \quad . \end{aligned} \quad (86)$$

We can solve the above equation w.r.t. $v = \frac{u}{\sqrt[3]{C}}$.²⁸

$$\begin{aligned} u_+ = \frac{1}{r_+^2} &= \sqrt[3]{C} \frac{(\sqrt{3}+1)\bar{\text{sn}}_+^2 - 2\sqrt{3}(1 - |\bar{\text{cn}}_+|)}{\bar{\text{sn}}_+^2}, \quad u_- = \frac{1}{r_-^2} = \sqrt[3]{C} \frac{(\sqrt{3}+1)\bar{\text{sn}}_-^2 - 2\sqrt{3}(1 - |\bar{\text{cn}}_-|)}{\bar{\text{sn}}_-^2}, \\ \bar{\text{sn}}_\pm(y, C, C') &\equiv \text{sn}(-\sqrt[4]{3}C^{1/6}(\pm 2y + C'), \frac{\sqrt{3}+1}{2\sqrt{2}}), \quad \bar{\text{cn}}_\pm(y, C, C') \equiv \text{cn}(-\sqrt[4]{3}C^{1/6}(\pm 2y + C'), \frac{\sqrt{3}+1}{2\sqrt{2}}). \end{aligned} \quad (87)$$

From the requirement $u = \frac{1}{r^2} > 0$, the above result says²⁹

$$\frac{\sqrt{3}-1}{\sqrt{3}+1} \leq |\bar{\text{cn}}_\pm(y, C, C')| = \left| \text{cn}(-\sqrt[4]{3}C^{1/6}(\pm 2y + C'), \frac{\sqrt{3}+1}{2\sqrt{2}}) \right| \leq 1 \quad . \quad (88)$$

We must choose C and C' in such a way that the above relation is valid for $\forall y \in (0, l)$. $r(y=0)$ and $\left. \frac{dr}{dy} \right|_{y=0}$ are related to C and C' as follows.

$$\begin{aligned} r(0) &= C^{-1/6} \frac{|\text{sn}0(C, C')|}{\{(\sqrt{3}+1)\text{sn}0(C, C')^2 - 2\sqrt{3}(1 - |\text{cn}0(C, C')|)\}^{1/2}} \quad , \\ \text{sn}0(C, C') &= \text{sn}(-\sqrt[4]{3}C^{1/6}C', \frac{\sqrt{3}+1}{2\sqrt{2}}) \quad , \quad \text{cn}0(C, C') = \text{cn}(-\sqrt[4]{3}C^{1/6}C', \frac{\sqrt{3}+1}{2\sqrt{2}}) \quad , \\ \left. \frac{dr}{dy} \right|_{y=0} &= \mp r(0)^3 \sqrt{C - \frac{1}{r(0)^6}} \quad , \\ r_+(l) &= C^{-1/6} \frac{|\bar{\text{sn}}_+(l, C, C')|}{\{(\sqrt{3}+1)\bar{\text{sn}}_+(l, C, C')^2 - 2\sqrt{3}(1 - |\bar{\text{cn}}_+(l, C, C')|)\}^{1/2}} \quad , \\ r_-(l) &= C^{-1/6} \frac{|\bar{\text{sn}}_-(l, C, C')|}{\{(\sqrt{3}+1)\bar{\text{sn}}_-(l, C, C')^2 - 2\sqrt{3}(1 - |\bar{\text{cn}}_-(l, C, C')|)\}^{1/2}} \quad . \end{aligned} \quad (89)$$

The two integration constants come from the second derivative differential equation (79). In the numerical approach of Runge-Kutta method, the constants are given by $r(y=0)$ and $\left. \frac{dr}{dy} \right|_{y=0}$. It is important to check, in the simple case of the flat model, that the numerical solution correctly produces the analytic one. In the warped case, we rely only on the numerical method.

²⁸ Note that one of two solutions (of a quadratic equation w.r.t. v) is omitted here because of $(\sqrt{3}+1)\bar{\text{sn}}^2 - 2\sqrt{3}(1 - |\bar{\text{cn}}|) = -\{(\sqrt{3}+1)|\bar{\text{cn}}| + \sqrt{3}-1\}\{|\bar{\text{cn}}|+1\} < 0$.

²⁹ Using the relation $\bar{\text{sn}}^2 = 1 - \bar{\text{cn}}^2$ we know $(\sqrt{3}+1)\bar{\text{sn}}^2 - 2\sqrt{3}(1 - |\bar{\text{cn}}|) = \{\sqrt{3}-1 - (\sqrt{3}+1)|\bar{\text{cn}}|\}\{|\bar{\text{cn}}|-1\}$.

10 Appendix B: Weight Function and Minimal Surface Curve

In Sec.7, we have presented a specification of the weight function $W(\tilde{p}, y)$. Here we examine its validity by numerically evaluating a consistency equation, given later, for each W appeared in (67).

10.1 B.1 Reciprocal Space

The 4D boundary manifold described in Sec.5 is characterized by the metric:

$$ds^2 = \left(\delta_{ab} + \frac{x^a x^b}{(r \frac{dr}{dy})^2} \right) dx^a dx^b \equiv g_{ab}(x) dx^a dx^b \quad , \quad r = \sqrt{x^a x^a} \quad , \quad (\delta_{ab}) = \text{diag}(1, 1, 1, 1) \quad ,$$

$$A = \int \sqrt{\det g_{ab}} d^4x = \int_{1/\Lambda}^l \sqrt{r'^2 + 1} r^3 dy \quad , \quad r' = \frac{dr}{dy} \quad , \quad (90)$$

where $\{x^a; a = 1, 2, 3, 4\}$ are the coordinates of the 4D Euclidean space manifold. We introduce the reciprocal coordinates $\{p^a\}$ defined by

$$x^a = \frac{p^a}{p^2} \quad , \quad p^2 \equiv p^a p^a \quad ,$$

$$p^a = \frac{x^a}{x^2} \quad , \quad x^2 \equiv x^a x^a \quad ,$$

$$x^2 = \frac{1}{p^2} \quad . \quad (91)$$

The metric (90) can be, in terms of these coordinates, rewritten as

$$dx^a = \frac{1}{p^2} (-\delta^{ab} + 2Q^{ab}) dp^b \quad , \quad Q^{ab} \equiv \delta^{ab} - \frac{p^a p^b}{p^2} \quad ,$$

$$Q^{ab} = Q^{ba} \quad , \quad p^a Q^{ab} = 0 \quad , \quad Q^{ab} p^b = 0 \quad , \quad Q^{ab} Q^{bc} = Q^{ac} \quad , \quad \delta^{ab} Q^{ab} = 3 \quad ,$$

$$ds^2 = \frac{1}{(p^2)^2} \left(\delta_{ab} + p^2 \frac{p^a p^b}{(\frac{dp}{dy})^2} \right) dp^a dp^b \equiv \hat{g}_{ab}(p) dp^a dp^b \quad , \quad \tilde{p} = \sqrt{p^a p^a} \quad . \quad (92)$$

The 4D volume (the area of the boundary surface) is given by

$$A = \int \sqrt{\det \hat{g}_{ab}} d^4p = \int \sqrt{1 + \frac{\tilde{p}^4}{(\frac{d\tilde{p}}{dy})^2}} \frac{d\tilde{p}}{\tilde{p}^5}$$

$$= \int_{1/\Lambda}^l \sqrt{(\frac{\tilde{p}'}{\tilde{p}^2})^2 + 1} \tilde{p}^{-3} dy \quad , \quad \tilde{p}' \equiv \frac{d\tilde{p}}{dy} \quad , \quad (93)$$

where the S^3 property: $\tilde{p} = 1/\sqrt{x^2} = r(y)^{-1} = \tilde{p}(y)$ is used. Λ is the UV-cutoff for the 4D momentum integral. The minimal area principle gives the equation.

$$\begin{aligned} \tilde{p}(y) &\rightarrow \tilde{p}(y) + \delta\tilde{p}(y) \quad , \quad \delta\mathcal{A} = 0 \quad , \\ 3 + \frac{(\tilde{p}''\tilde{p} - 2\tilde{p}'^2)/\tilde{p}^4}{1 + (\tilde{p}'/\tilde{p}^2)^2} &= 0 \quad \text{or} \quad \frac{d^2\tilde{p}}{dy^2} + \frac{1}{\tilde{p}}\left(\frac{d\tilde{p}}{dy}\right)^2 + 3\tilde{p}^3 = 0 \quad . \end{aligned} \quad (94)$$

This result is the same as (60) expressed by $r(=1/\tilde{p})$.

10.2 B.2 Numerical Confirmation of the Relation between Weight Function and Minimal Surface Curve

The dominant configuration (path, $\tilde{p} = \tilde{p}(y)$) to the Casimir energy (67) is given by the ordinary variation method (minimal "action" principle).

$$\begin{aligned} y \rightarrow y + \delta y \quad , \quad \delta\{W(\tilde{p}(y), y)\tilde{p}^3(y)F(\tilde{p}(y), y)\} &= \delta y\left(\frac{d\tilde{p}}{dy}\frac{\partial}{\partial\tilde{p}} + \frac{\partial}{\partial y}\right)(\tilde{p}^3W(\tilde{p}, y)F(\tilde{p}, y)) = 0 \quad , \\ \frac{d\tilde{p}}{dy} &= \frac{-\frac{\partial\ln(WF)}{\partial y}}{\frac{3}{\tilde{p}} + \frac{\partial\ln(WF)}{\partial\tilde{p}}} \quad , \end{aligned} \quad (95)$$

where $W(\tilde{p}, y)$ is the weight function 'practically' introduced in Sec.6 and is properly defined in Sec.7 using 5D coordinates (r, y) . In this subsection we define $W(\tilde{p}, y)$ using (\tilde{p}, y) . $F(\tilde{p}, y)$ is given in (49). The coordinate version of the above result is given in the text (71). We can also obtain $d^2\tilde{p}/dy^2$.

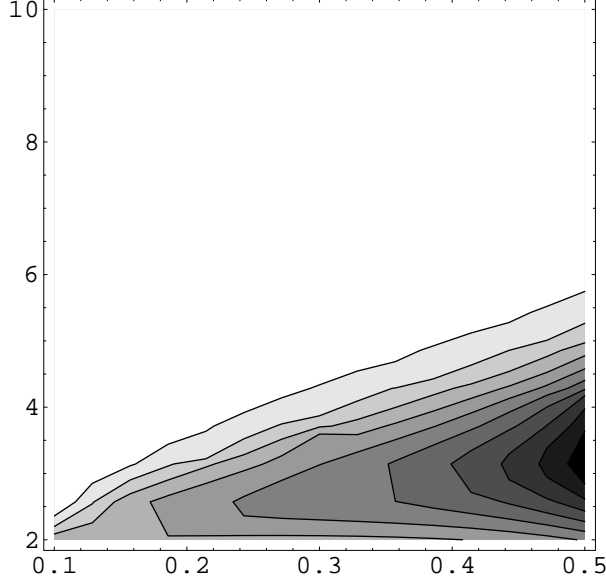
$$\begin{aligned} \mathcal{W}_y &\equiv \partial_y \ln(WF) \quad , \quad \mathcal{W}_{\tilde{p}} \equiv \partial_{\tilde{p}} \ln(WF) \quad , \\ \frac{d\tilde{p}}{dy} &= -\frac{\mathcal{W}_y}{3\tilde{p}^{-1} + \mathcal{W}_{\tilde{p}}} \equiv \mathcal{V}_1(W, \partial_{\tilde{p}}W, \partial_yW; \tilde{p}, y) \quad , \\ \frac{d^2\tilde{p}}{dy^2} &= -\frac{\partial_y\mathcal{W}_y}{3\tilde{p}^{-1} + \mathcal{W}_{\tilde{p}}} + \frac{\mathcal{W}_y(\partial_{\tilde{p}}\mathcal{W}_y + \partial_y\mathcal{W}_{\tilde{p}})}{(3\tilde{p}^{-1} + \mathcal{W}_{\tilde{p}})^2} - \frac{\mathcal{W}_y^2(-3\tilde{p}^{-2} + \partial_{\tilde{p}}\mathcal{W}_{\tilde{p}})}{(3\tilde{p}^{-1} + \mathcal{W}_{\tilde{p}})^3} \\ &\equiv \mathcal{V}_2(W, \partial_{\tilde{p}}W, \partial_yW, \partial_{\tilde{p}}^2W, \partial_y\partial_{\tilde{p}}W, \partial_y^2W; \tilde{p}, y) \quad . \end{aligned} \quad (96)$$

Note that the RHSs of the expressions $d\tilde{p}/dy$ and $d^2\tilde{p}/dy^2$ above are functions of \tilde{p} and y . If we consider $W(\tilde{p}, y)$ is unknown, by inserting the above ones in (94), we obtain a partial differential equation for $W(\tilde{p}, y)$ involving up to 2nd derivative. We call it "W-defining equation".

$$\text{W-defining Equation :} \quad \mathcal{V}_2 + \frac{1}{\tilde{p}}\mathcal{V}_1^2 + 3\tilde{p}^3 = 0 \quad , \quad (97)$$

where \mathcal{V}_1 and \mathcal{V}_2 are defined in (96). We consider that the 2nd-derivative differential equation defines the weight function $W(\tilde{p}, y)$. It is difficult to solve it. Here we are content with a numerical consistency check.

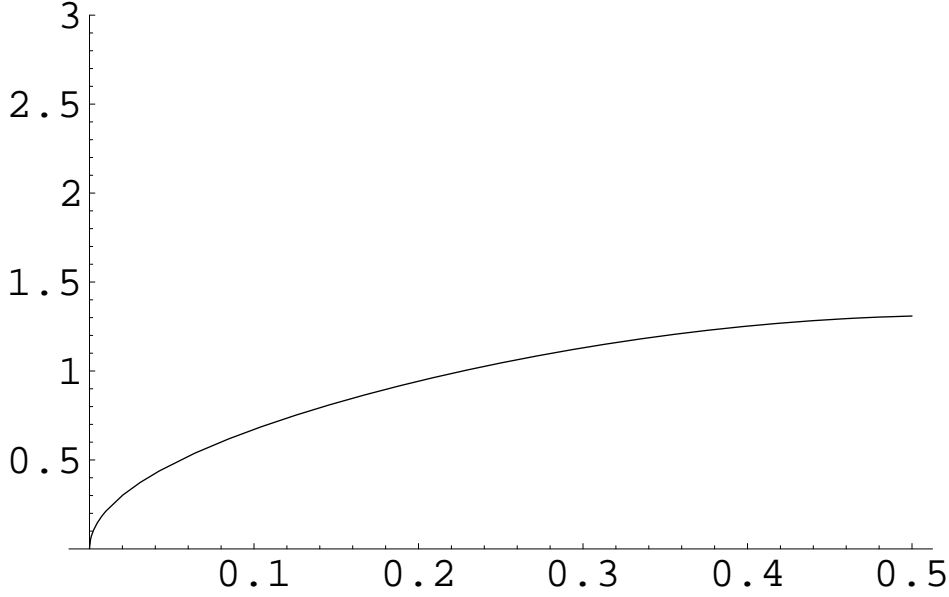
Figure 20: Contour of $\tilde{p}^3 W_6(\tilde{p}, y) F(\tilde{p}, y)$ (parabolic suppression2, Fig.15). $\Lambda = 10$, $l = 0.5$. Horizontal axis: $1.001/\Lambda \leq y \leq 0.99999l$, Vertical Axis: $1/l \leq \tilde{p} \leq \Lambda$.



If we take some example of $W(\tilde{p}, y)$ appearing in (67), the dominant configuration $\tilde{p}_W = \tilde{p}_W(y)$ is graphically shown by the valley bottom line of the Casimir energy integrand $W(\tilde{p}, y)\tilde{p}^3 F(\tilde{p}, y)$. (See Fig.12-15) On the other hand there exists another path $\tilde{p}_g(y)$ which is the minimal surface curve of the bulk geometry, (60) or (94). $\tilde{p}_g(y)$ is determined by the 5D metric, and is completely independent of both the weight W and the model F .³⁰ The W -defining equation above represents the equality: $\tilde{p}_W(y) = \tilde{p}_g(y)$. We can numerically compare $\tilde{p}_W(y)$ and $\tilde{p}_g(y)$. We show, in Fig.20, the contour of Fig.15 (Parabolic Suppression W6). We can see the valley-bottom line as $\tilde{p}_W(y) \approx 4.3\sqrt{y}$. In Fig.21, we show the minimal surface curve $\tilde{p}_g(y) = 1/r_g(y)$ which is $r_-(y)$ solution with $C = 5.1215$ and $C' = 1.068$ in (87) of App.A.2. The two graphs are similar, at least in the shape and the magnitude order. For other weights, we confirm similar situation.

³⁰ Precisely saying, the boundary conditions at $y = 0$ and $y = l$ (boundary values: $\tilde{p}(0)$ and $\tilde{p}(l)$) are also necessary.

Figure 21: Minimal Surface Curve $1/r_-(y)$, $C = 5.1215$, $C' = 1.068$ in (87). Horizontal axis: $0 \leq y \leq 0.5$, Vertical Axis: $0 \leq 1/r_- \leq 3$.



11 Appendix C: Numerical Evaluation of Scaling Laws: E_{Cas} (52), E_{Cas}^{RS} (55), and E_{Cas}^W (68)

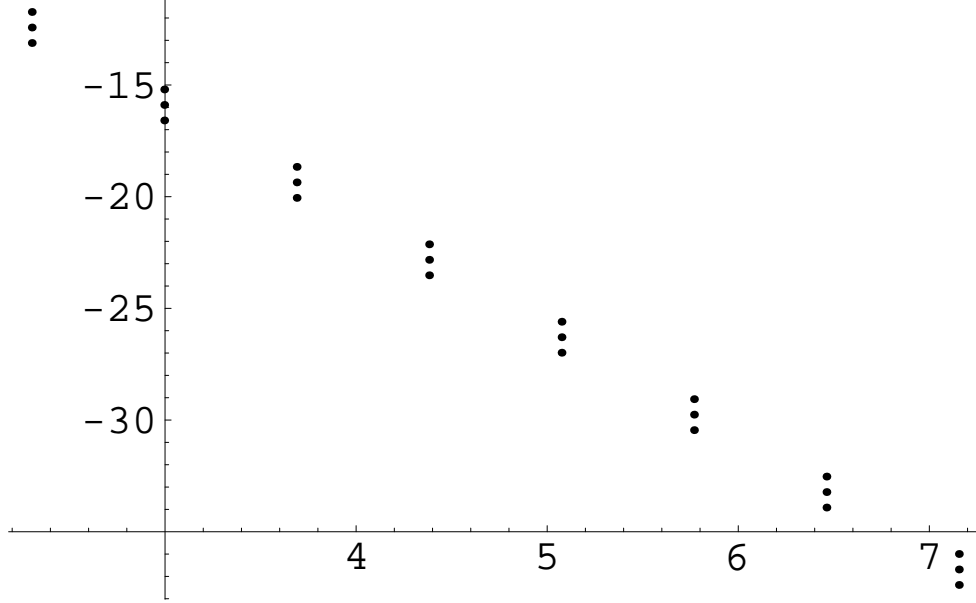
In the text, (regularized) Casimir energy is numerically calculated in three ways: 1) Original version (Rectangle-region integral), 2) Restricted-region integral (Randall-Sundrum type), 3) Weighted version. The final expressions show the *scaling* behaviors about the boundary (extra-space) parameter l and the 4D momentum cut-off Λ . The results are crucial for the present conclusion. Hence we explain here how the numerical results are obtained.

First, let us take the un-weighted case with the rectangle integral-region (original form) of Casimir energy (49).

$$2^3 \pi^2 E_{Cas}(\Lambda, l) = \int_{1/l}^{\Lambda} d\tilde{p} \int_{1/\Lambda}^l dy \tilde{p}^3 F(\tilde{p}, y) \quad , \quad (98)$$

where $\tilde{p}^3 F(\tilde{p}, y)$ is explicitly given in (51). The integral region is graphically shown, in Fig.1, as the rectangle ($\epsilon = 1/\Lambda$, $\mu = 1/l$). The graphs of the integrand of (98), $\tilde{p}^3 F(\tilde{p}, y)$, are shown for $(l, \Lambda) = (1, 10)$ [Fig.2], $(1, 100)$ [Fig.3], $(1, 1000)$ [Fig.4], in the text. From the behaviors we can expect $E_{Cas}(\Lambda, l)$, (98), leadingly behaves as $l\Lambda^5$, because the depth of the valley's, shown in Fig.2-4, proportional to Λ^4 and their behaviors are monotonous (except near the boundaries $y = 1/\Lambda$ and l). It is confirmed by directly evaluating (98) numerically (the numerical integral in [29]). We plot the numerical results for various Λ and l in Fig.22. From the straight-line behavior we can safely fit the curve as $2^3 \pi^2 E_{Cas} = l\Lambda^5(a_5 + b_5 \ln(l\Lambda))$.

Figure 22: Casimir Energy E_{Cas} of (98) for various (Λ, l) . Horizontal axis: $\ln \Lambda$ ($\Lambda = 10, 20, 40, \dots, 1280$), Vertical Axis: $-\ln(|2^3 \pi^2 E_{Cas}|)$. The results are grouped to three lines. The values placed on the top, middle and bottom lines correspond to $l = 10, 20$ and 40 respectively.



The best fit is given by (Manipulating Numerical Data in [29])

$$2^3 \pi^2 E_{Cas}(\Lambda, l) = -0.1249 \, l \Lambda^5 - (1.41, 0.706, 0.353) \times 10^{-5} \, l \Lambda^5 \ln(l\Lambda) \quad . \quad (99)$$

The triplet results corresponds to $l = 10, 20$ and 40 . The first term is firmly fixed (the valid figures are 4 digits), whereas the second one is unstable (the coefficients are proportional to $1/l$). The second one is numerically tiny compared with the first, and its determination requires more careful treatment of small numbers. To determine it firmly, calculation using larger values of Λ and l are necessary.

For the restricted region case, (55), we do the numerical integral of the following expression.

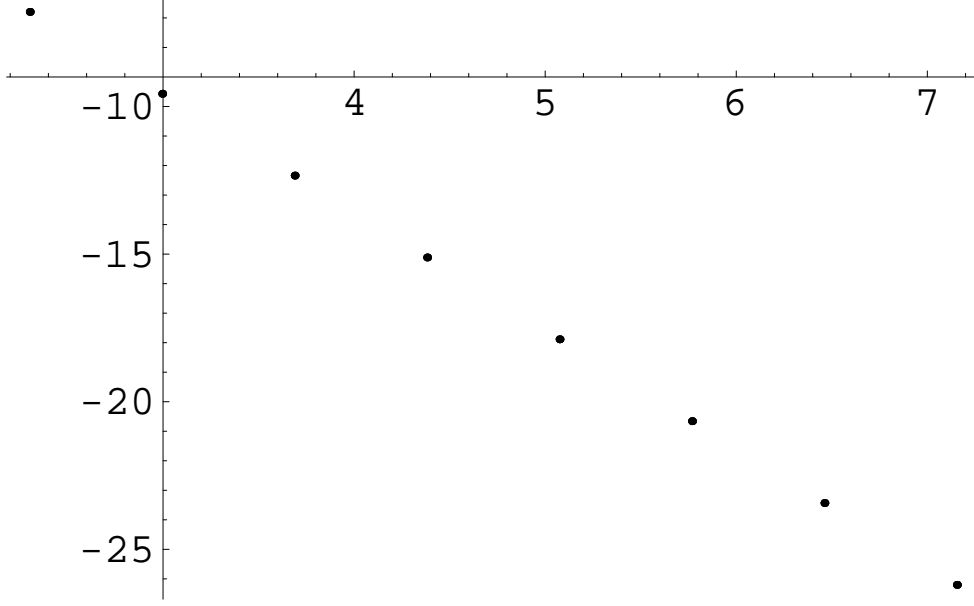
$$2^3 \pi^2 E_{Cas}^{RS} = \int_{1/l}^{\Lambda} dq \int_{1/\Lambda}^{1/q} dy \, q^3 F(q, y) = \int_{1/\Lambda}^l du \int_{1/l}^{1/u} d\tilde{p} \, \tilde{p}^3 F(\tilde{p}, u) \quad . \quad (100)$$

We plot the results, in Fig.23, for various Λ and l . From the straight line behavior, we can safely fit the curve as $2^3 \pi^2 E_{Cas}^{RS} = \Lambda^4 (a_4 + b_4 \ln(l\Lambda))$. The best fit is given by

$$2^3 \pi^2 E_{Cas}^{RS}(\Lambda, l) = -8.93814 \times 10^{-2} \, \Lambda^4 + (+7.73, -4.83, +5.00) \times 10^{-10} \, \Lambda^4 \ln(l\Lambda) \quad . \quad (101)$$

The triplet results corresponds to $l = 10, 20$ and 40 . The first term is firmly fixed (the valid figures are 6 digits), whereas the second one is unstable. The second one is numerically

Figure 23: Casimir Energy E_{Cas}^{RS} of (100) for variou (Λ, l) . Horizontal axis: $\ln \Lambda$ ($\Lambda = 10, 20, 40, \dots, 1280$), Vertical Axis: $-\ln(|2^3 \pi^2 E_{Cas}^{RS}|)$. The results are placed on a straight line for different Λ 's and overlap (within the presented dots) for three different values of $l = 10, 20$ and 40 .



very tiny compared with the first, and we may say that the second term vanishes within the present numerical precision.

Finally we explain the weighted case (67) taking the elliptic type, W_1 , as an example.

$$2^3 \pi^2 E_{Cas}^{W_1}(\Lambda, l) = \int_{1/l}^{\Lambda} d\tilde{p} \int_{1/\Lambda}^l dy \tilde{p}^3 W_1(\tilde{p}, y) F(\tilde{p}, y) \quad ,$$

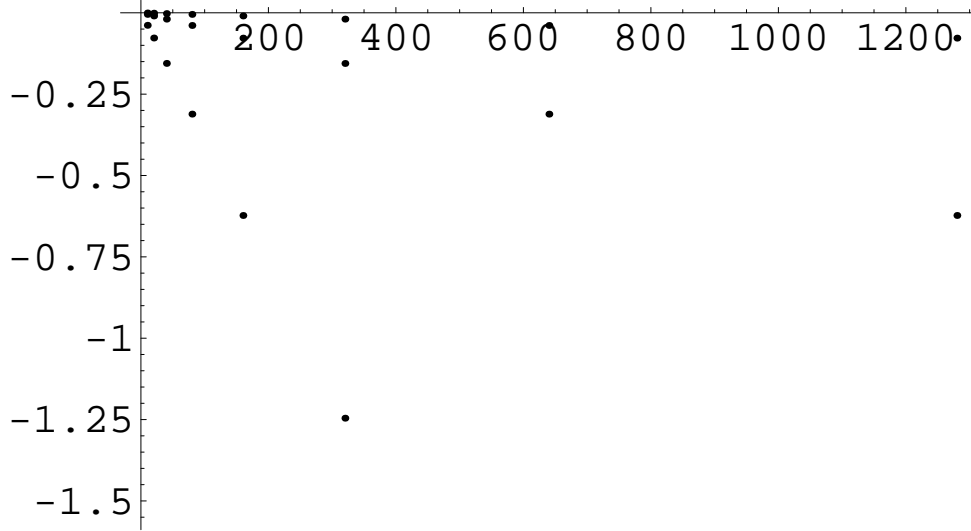
$$W_1(\tilde{p}, y) = e^{-\frac{l^2}{2} \tilde{p}^2 - \frac{1}{2l^2} y^2} \quad , \quad (102)$$

where UV cut-off Λ and IR cut-off l are introduced to see the scaling behavior. In Fig.24, we show the numerical results of $E_{Cas}^{W_1}(\Lambda, l)$ for different Λ and l . (Note that the axes of Fig.24 are linear scale, not log-scale.) From the straight line behavior of Fig.24, we can safely fit the curve as $2^3 \pi^2 E_{Cas}^{W_1} = (\Lambda/l)(a_1 + b_1 \ln(l\Lambda))$. The best fit is given by

$$2^3 \pi^2 E_{Cas}^{W_1}(\Lambda, l) = -(3.892, 3.894, 3.894) \frac{\Lambda}{l^3} + (-0.221, 1.70, 1.76) \times 10^{-4} \frac{\Lambda \ln(l\Lambda)}{l^3} \quad . \quad (103)$$

The triplet results corresponds to $l = 10, 20$ and 40 . The first term is firmly fixed (the valid figures are 3 digits at least), whereas the second one is unstable. This data shows the coefficients become stable as we increase l . As for other types of W 's, the best fit scaling behaviors are listed in (68) of the text. W_2 and W_3 do not well suppress the UV-divergences.

Figure 24: Casimir Energy $E_{Cas}^{W_1}$ of (102) for various (Λ, l) . Horizontal axis: Λ ($\Lambda = 10, 20, 40, \dots, 1280$), Vertical Axis: $2^3 \pi^2 E_{Cas}^{W_1}$. The results are grouped to three lines. The values placed on the top, middle and bottom lines correspond to $l = 40, 20$ and 10 respectively.



12 Acknowledgement

Parts of the content of this work have been already presented at the workshop "Evolution of Space-Time-Matter in the Early Universe" (07.5.29, Univ. of Tokyo, Japan), ICGA8 (07.8.29-9.1, Nara Women's Univ., Japan), 62th Japan Physical Society Meeting (07.9.21-24, Hokkaido Univ., Sapporo, Japan), KIAS-YITP joint workshop "Strings, Cosmology and Phenomenology" (07.9.24-28, Kyoto Univ., Japan), the workshop "Higher Dimensional Gauge Theory and the Unification of Forces" (07.11.29-30, Kobe Univ., Japan) and the workshop "Progress of String Theory and Quantum Field Theory" (07.12.7-10, Osaka City Univ.). The author thanks T. Inagaki (Hiroshima Univ.), K. Ito (TIT), T. Kawano (Univ. of Tokyo), M. Peskin (SLAC) and T. Yoneya (Univ. of Tokyo) for useful comments and discussions on the occasions. He also thanks T. Tamaribuchi (Shizuoka Univ.) for the advice in the computer calculation.

References

- [1] Th. Kaluza, Sitzungsberichte der K.Preussischen Akademie der Wissenschaften zu Berlin. p966 (1921)
- [2] O. Klein, Z. Physik **37** 895 (1926)

- [3] T. Appelquist and A. Chodos, Phys.Rev.**D28**(1983)772
T. Appelquist and A. Chodos, Phys.Rev.Lett.**50**(1983)141
- [4] M. Bordag, U. Mohideen and V.M. Mostepanenko, Phys.Rept.**353**(2001),1,quant-ph/0106045
- [5] N. Arkani-Hamed, A.G. Cohen and H. Georgi, Phys.Rev.Lett.**86**(2001)4757, hep-th/0104005
- [6] C.T. Hill, S. Pokorski and J. Wang, Phys.Rev.**D64**(2001)105005, hep-th/0104035
- [7] F. Bauer, M. Lindner and G. Seidl, JHEP**0405**(2004)026, hep-th/0309200
- [8] L. Randall, M.D. Schwartz and S. Thambyahpillai, JHEP**0510**(2005)110, hep-th/0507102
- [9] L. Randall and M.D. Schwartz, JHEP **0111** (2001) 003, hep-th/0108114
- [10] S. Ichinose and A. Murayama, Phys.Rev.**D76**(2007)065008, hep-th/0703228,
- [11] S. Ichinose, "Casimir and Vacuum Energy of 5D Warped System and Sphere Lattice Regularization", Proc. of VIII Asia-Pacific Int. Conf. on Gravitation and Astrophysics (ICGA8,Aug.29-Sep.1,2007,Nara Women's Univ.,Japan),edited by M. Kenmoku and M. Sasaki,p36, arXiv:/0712.4043
- [12] S. Ichinose, Int.Jour.Mod.Phys.23A(2008)2245, Proc. of the Int. Conf. on Prog. of String Theory and Quantum Field Theory (Dec.7-10,2007,Osaka City Univ.,Japan),edited by K. Fujiwara et al, arXiv:/0804.0945
- [13] D.Z. Freedman, S.D. Mathur, A. Matusis and L. Rastelli, Nucl.Phys.**B546**(1999)96, hep-th/9804058
- [14] M. Henningson and K. Skenderis, JHEP **9807**(1998)023, hep-th/9806087
- [15] J. Distler and F. Zamora, Adv.Theor.Math.Phys.**2**(1999)1405, hep-th/9810206
- [16] L. Girardello, M. Petrini, M. Porrati and A. Zaffaroni, JHEP **9812**(1998)022, hep-th/9810126
- [17] M. Porrati and A. Starinets, Phys.Lett.**B454**(1999)77, hep-th/990385
- [18] D.Z. Freedman, S.S. Gubser, K. Pilch and N.P. Warner, Adv.Theor.Math.Phys.**3**(1999)363, hep-th/9904017
- [19] Y. Nambu, "Duality and hydrodynamics", Lecture notes at the Copenhagen symposium (unpublished), 1970
- [20] T. Goto, Prog.Theor.Phys.**46**(1971),1560

- [21] A.M. Polyakov, Phys.Lett.**103B**(1981),207
- [22] S. Ichinose, Phys.Lett.**152B**(1985),56
- [23] J. Schwinger, Phys.Rev.**82**(1951)664
- [24] P.A.M. Dirac, "The Principles of Quantum Mechanics", 4th Edition, Oxford Univ. Press, Oxford, 1958
- [25] E.A. Mirabelli and M.E. Peskin, Phys.Rev.**D58**(1998)065002, hep-th/9712214
- [26] S. Ichinose and A. Murayama, Nucl.Phys.**B710**(2005)255, hep-th/0401011
- [27] R.P. Feynman, "Statistical Mechanics", W.A.Benjamin,Inc., Massachusetts, 1972
- [28] T. Yoneya, *Duality and Indeterminacy Principle in String Theory* in "Wandering in the Fields", eds. K. Kawarabayashi and A. Ukawa (World Scientific,1987), p.419
T. Yoneya, *String Theory and Quantum Gravity* in "Quantum String Theory", eds. N. Kawamoto and T. Kugo (Springer,1988), p.23
T. Yoneya, Prog.Theor.Phys.**103**(2000)1081
- [29] S. Wolfram, **The Mathematica Book**, 4th ed., Wolfram Media/Cambridge University Press, c1999